Water Resources Research

RESEARCH ARTICLE
10.1029/2022WR034114

Athabasca River Avulsion Underway in the Peace-Athabasca Delta, Canada

Bo Wang[1,2], Laurence C. Smith[1,2], Colin Gleason[3], Ethan D. Kyzivat[1,2], Jessica V. Fayne[4], Merritt E. Harlan[3], Theodore Langhorst[5], Dongmei Feng[6], Emily Eidam[7], Sebastian Munoz[1,2], Julianne Davis[5], Tamlin M. Pavelsky[5], and Daniel L. Peters[8]

[1]Institute at Brown for Environment and Society, Brown University, Providence, RI, USA, [2]Department of Earth, Environmental & Planetary Sciences, Brown University, Providence, RI, USA, [3]Department of Civil and Environmental Engineering, University of Massachusetts Amherst, Amherst, MA, USA, [4]Department of Earth and Environmental Sciences, University of Michigan, Ann Arbor, MI, USA, [5]Department of Earth, Marine and Environmental Sciences, University of North Carolina at Chapel Hill, Chapel Hill, NC, USA, [6]Department of Chemical and Environmental Engineering, University of Cincinnati, Cincinnati, OH, USA, [7]College of Earth, Ocean, and Atmospheric Sciences, Oregon State University, Corvallis, OR, USA, [8]Watershed Hydrology & Ecology Research Division, Environment Climate Change Canada, Victoria, BC, Canada

Abstract Avulsions change river courses and transport water and sediment to new channels impacting infrastructure, floodplain evolution, and ecosystems. Abrupt avulsion events (occurring over days to weeks) are potentially catastrophic to society and thus receive more attention than slow avulsions, which develop over decades to centuries and can be challenging to identify. Here, we examine gradual channel changes of the Peace-Athabasca River Delta (PAD), Canada using in situ measurements and 37 years of Landsat satellite imagery. A developing avulsion of the Athabasca River is apparent along the Embarras River–Mamawi Creek (EM) distributary. Its opening and gradual enlargement since 1982 are evident from multiple lines of observation: Between 1984 and 2021 the discharge ratio between the EM and the Athabasca River more than doubled, increasing from 9% to 21%. The EM has widened by +53% since 1984, whereas the Athabasca River channel width has remained stable. The downstream Mamawi Creek delta is growing at a discharge-normalized rate roughly twice that of the Athabasca River delta in surface area. Longitudinal global navigation satellite systems field surveys of water surface elevation reveal the EM possesses a ~2X slope advantage (8×10^{-5} vs. 4×10^{-5}) over the Athabasca River, and unit stream power and bed shear stress suggest enhanced sediment transport and erosional capacity through the evolving flow path. Our findings: (a) indicate that a slow avulsion of the Athabasca River is underway with potentially long-term implications for inundation patterns, ecosystems, and human use of the PAD; and (b) demonstrate an observational approach for identifying other slow avulsions at river bifurcations globally.

Plain Language Summary Avulsions shift river courses and move water and sediment to new channels, which affect infrastructure, floodplains, and ecosystems. Slow avulsions take decades to develop and are more difficult to identify. Using on-the-ground measurements and 37 years of Landsat satellite imagery, we analyze gradual channel changes in the Peace-Athabasca River Delta (PAD), Canada. The Athabasca River is changing course such that more of its water enters its westernmost outlet, the Embarras River–Mamawi Creek (EM) channel. Multiple lines of evidence demonstrate that the EM channel has been gradually opening since 1982. Between 1984 and 2021, the water entering the EM channel increased from 9% to 21% of the river's total flow. Since 1984, the EM channel has widened by 53%, while the Athabasca River channel has remained stable. The delta forming at the EM mouth (i.e., Mamawi Creek delta) has grown twice as fast as the Athabasca River delta. Field measurements of water surface elevation show the slope of the EM channel is twice as steep as the slope of the lower Athabasca River (8×10^{-5} vs. 4×10^{-5}). Because water tends to flow down the steepest slope, we expect more water to flow down the EM channel in the future. Our findings indicate a slow capture of Athabasca River water into its EM channel, with potential long-term implications for the delta's inundation pattern, ecosystems, and traditional Indigenous activities.

Key Points:

- We assess a potential avulsion of the Athabasca River in the Peace-Athabasca Delta, Canada using field measurements and remote sensing
- Analysis of hydrological and morphological observations affirm that a slow avulsion is currently underway
- The avulsion may accelerate in the future and cause transformative effects on the delta's vegetation, habitat, and ecosystems

Supporting Information:

Supporting Information may be found in the online version of this article.

Correspondence to:

B. Wang,
bo_wang1@brown.edu

Citation:

Wang, B., Smith, L. C., Gleason, C., Kyzivat, E. D., Fayne, J. V., Harlan, M. E., et al. (2023). Athabasca River avulsion underway in the Peace-Athabasca Delta, Canada. *Water Resources Research*, *59*, e2022WR034114. https://doi.org/10.1029/2022WR034114

Received 14 NOV 2022
Accepted 15 FEB 2023

Author Contributions:

Conceptualization: Bo Wang, Laurence C. Smith
Funding acquisition: Laurence C. Smith
Investigation: Bo Wang, Colin Gleason, Ethan D. Kyzivat, Jessica V. Fayne, Merritt E. Harlan, Theodore Langhorst, Dongmei Feng, Emily Eidam, Tamlin M. Pavelsky, Daniel L. Peters
Methodology: Bo Wang, Laurence C. Smith
Software: Bo Wang
Writing – original draft: Bo Wang
Writing – review & editing: Laurence C. Smith, Colin Gleason, Ethan D. Kyzivat, Jessica V. Fayne, Merritt E. Harlan, Theodore Langhorst, Dongmei Feng, Emily Eidam, Sebastian Munoz, Julianne Davis, Tamlin M. Pavelsky, Daniel L. Peters

1. Introduction

An avulsion is the abandonment of a river channel and the formation of a new channel at a lower elevation of the floodplain (J. R. L. Allen, 1965). It is a normal and vital process in the formation of multi-channel rivers, floodplains, and alluvial basins (Fisk, 1944; Mohrig et al., 2000; Slingerland & Smith, 2004; Sun et al., 2002). Avulsions reroute water and sediment across existing floodplains, in some cases leading to the creation of new floodplains along previously unoccupied flow paths (Roberts et al., 2003; Rosen & Xu, 2013; L. C. Smith, 2020; N. D. Smith et al., 1989, 1998; Zhang & Fang, 2017). For example, avulsion of the Saskatchewan River (Canada) replaced over 500 km^2 of wetlands with anabranching channels, splay complexes, and small lakes (N. D. Smith et al., 1989, 1998), avulsion of the Taquari River (Brazil) changed ecosystem services in the Brazilian Pantanal wetlands (Louzada et al., 2021), and avulsions of the Yellow River (China) are intimately linked to socioeconomic developments in Chinese history (Chen et al., 2012). Avulsions, therefore, can have major impacts on landforms, ecosystems, and human societies.

Causal factors of avulsions have been well studied. Topographic slope (i.e., gradient) advantage of a prospective new river course is necessary for an avulsion to occur (Ethridge et al., 1999; Jones & Schumm, 1999; Slingerland & Smith, 1998). Modeling investigations demonstrate that a potential avulsion course (e.g., a new flow path through a levee crevasse) having a slope ~4X steeper than the main-channel slope is likely to trigger an avulsion (Slingerland & Smith, 1998). From field studies, ongoing channel avulsions can be associated with even smaller slope advantages, for example, just 1.2 to 1.5X the main channel slope in low-relief deltaic environments (Phillips, 2012; Wang et al., 2020). Jones and Schumm (1999) reviewed various factors that can increase the ratio of a potential avulsion course slope (S_a) to existing channel slope (S_e) through decreased S_e or increased S_a. Decreased S_e can be caused by increased sinuosity, downstream aggradation, or tectonic uplift of the existing channel, while increased S_a typically results from development of an alluvial ridge. Such processes decrease river channel stability and increase the probability of avulsion forming (Jones & Schumm, 1999).

In addition to topographic slope, other factors influencing river avulsion include substrate composition, abandoned channels, vegetation, bank cohesion, and floodplain width (Aslan et al., 2005; Gradziński et al., 2003; Makaske et al., 2012; Nanson & Knighton, 1996). In multi-thread anabranching rivers, stable cohesive banks and vegetation are favorable preconditions for channel avulsion (Gradziński et al., 2003; Nanson & Knighton, 1996). In the meandering Mississippi River, avulsions are rare despite widespread slope advantages—an avulsion at the Mississippi-Atchafalaya diversion was more likely driven by an erodible substrate and presence of abandoned floodplain channels available for reoccupation (Aslan et al., 2005). The importance of easily erodible substrates and relict channels (in addition to a slope advantage) is reported in many other avulsion sites (Ethridge et al., 1999; Makaske et al., 2012; Mohrig et al., 2000; N. D. Smith et al., 1989).

Avulsion processes are widely studied through field measurements (Mohrig et al., 2000; N. D. Smith et al., 1989, 2014; Tornqvist, 1994), modeling (Chadwick et al., 2020; Jerolmack & Paola, 2007; Kleinhans et al., 2008; Ratliff et al., 2021; Slingerland & Smith, 1998; Törnqvist & Bridge, 2002), and laboratory experiments (Ashworth et al., 2004; Bryant et al., 1995; Edmonds et al., 2009; Ganti et al., 2016). Useful field data for the study of channel avulsion include river discharge (Lauzon & Murray, 2022; Mackey & Bridge, 1995), river stage (Wang & Xu, 2018; Wang et al., 2020), water surface slope (WSS) (Jones & Schumm, 1999; Prasojo et al., 2022), water depth (Bryant et al., 1995), channel width (Buehler et al., 2011), sediment cores (Donselaar et al., 2013; N. D. Smith et al., 1989; Tornqvist, 1994), and estimates of stream power and/or shear stress (Edmonds et al., 2009; Hajek & Edmonds, 2014; Slingerland & Smith, 2004; Yochum et al., 2017).

Satellite remote sensing is also an important tool used to study river avulsions (Brooke et al., 2022; Buehler et al., 2011; Iacobucci et al., 2020; Li et al., 2018; Lombardo, 2016; Valenza et al., 2020). DEMs and topographic maps are often used to calculate ratios between cross-valley and down-valley gradients (Aslan et al., 2005; Phillips, 2009; Sinha et al., 2014). Examples using Landsat imagery: Buehler et al. (2011) found decreasing channel widths from 1996 to 2008 downstream of an avulsion node; Rosen and Xu (2013) reported rapid growth of the Atchafalaya-Wax Lake delta due to a potential avulsion of the Atchafalaya River; Lombardo (2016) discovered that 29 out of 41 crevasses along tributaries of the Rio Mamaore led to avulsions; Edmonds et al. (2016) demonstrated that avulsion courses are controlled by floodplain topography; Brooke et al. (2022) documented 113 avulsions over the past 50 years and indicate three distinct controls on avulsion locations. Other Landsat-based studies include mapping of avulsion styles (i.e., incisional vs. depositional) and floodplain disturbance (Valenza et al., 2020), crevasse splays (Iacobucci et al., 2020), and paleochannels (Weissmann et al., 2015).

Avulsions can occur abruptly over a period of days to weeks (Qian, 1990; Sinha, 2009; N. D. Smith et al., 1989) or take decades to centuries to complete (Fisk, 1944; Jones & Harper, 1998; Schumm et al., 1996; Stouthamer & Berendsen, 2001; Tornqvist, 1994). The aforementioned studies focused mainly on the examination of avulsions' control factors, locations, and floodplain impacts. However, monitoring slow, ongoing avulsions through field and remote sensing observations is uncommon. Such studies can improve our understanding of avulsion processes, floodplain and/or delta evolution, and current and future impacts of river avulsions on ecosystems, infrastructure, and local communities.

An outstanding example of this is found within the Peace-Athabasca Delta (PAD), Canada (Figure 1), where (a) a major Athabasca River avulsion was narrowly averted in 1972 through a deliberately engineered cutoff through a meander bend (Bayrock & Root, 1972); and (b) the Embarras River, a large distributary of the Athabasca R., avulsed abruptly into the adjacent Mamawi Creek in 1982. Nearly two-thirds of the Embarras discharge now flows through this recently formed pathway (K. Timoney & Lee, 2016), and at least one study has linked it to altered PAD flooding patterns (Kay et al., 2019). Although this Embarras River–Mamawi Creek (EM) pathway opened some 40 years ago, it remains uncertain if the Athabasca River will fully avulse through the EM into Mamawi Lake (Figure 1). Should it do so, the avulsion would have transformative hydrological, ecological, and social impacts on the PAD.

Here, we merge field measurements and remote sensing to assess the status of a potential avulsion of the Athabasca River through the EM pathway which first opened in 1982. To do this, we: (a) analyze long-term hydrological data from the Water Survey of Canada along the EM watercourse and the Athabasca River mainstem; (b) analyze long-term changes of channel width and bar morphology along both flow paths using 37 years of archived Landsat satellite imagery processed in Google Earth Engine; (c) calculate surface area changes of downstream deltas in Mamawi Lake and Lake Athabasca; (d) present and interpret novel longitudinal profiles of in situ water surface elevation (WSE), water depth, and discharge collected in 2018 along the Athabasca River, Embarras River, and Mamawi Creek; and (e) calculate unit stream power and bed shear stress along both flow paths from these field measurements. We conclude that the Athabasca-Embarras-Mamawi flow path is indeed an active ongoing avulsion site and recommend that it be closely monitored to inform the protection and management of the PAD, as well as to provide the international scientific community with an example of an ongoing case study.

2. Study Area

The PAD is located at the confluence of the Peace, Athabasca, and Birch Rivers at the west end of Lake Athabasca in northeastern Alberta, Canada (Figure 1). It began forming about 10,000 years ago, has experienced major lobe-forming avulsions (D. G. Smith, 1994). Today it covers some ~6,000 km^2 in area. The PAD continuously receives relatively large infusions of water and sediment from the Athabasca River (Pavelsky & Smith, 2008, 2009), and occasionally receives Peace River water during ice-jam floods and extreme flows events (Bayrock & Root, 1972; Beltaos, Prowse, Bonsal, et al., 2006; Peters et al., 2006; Prowse & Lalonde, 1996). Beaver dams, above-average precipitation, wind seiches, and spring and summer floods are also agents of water recharge to floodplain basins (K. P. Timoney, 2021). The PAD is one of the world's largest and most productive inland freshwater deltas and is home to abundant populations of birds, waterfowl, fish, muskrat, beaver, moose, and wood bison (Prowse & Lalonde, 1996; K. Timoney, 2013). It was designated a RAMSAR wetland of international importance in 1982 and a 80% within the Wood Buffalo National Park which is a UNESCO World Heritage Site since 1983. The region is home to the Athabasca-Chipewyan, Mikisew Cree, and Métis Indigenous peoples, who rely on the PAD ecosystem for traditional hunting, fishing, trapping, and cultural activities.

The PAD has experienced several wetting and drying periods since the mid-1970s, with local residents noticing severe disturbance to wildlife and vegetation during the latter (see examples in K. Timoney, 2002). Previous research attributed the extended drying periods in the Peace Delta to reduced ice-jam flooding along the lower Peace River (Beltaos, Prowse, & Carter, 2006; Prowse & Conly, 1998; Prowse & Lalonde, 1996; D. G. Smith, 2003; Toyra et al., 2002; Wolfe et al., 2006). Reduced frequency of ice-jam floods is expected in the future under climate-related projections (Beltaos, 2023). In the Athabasca Delta, Kay et al. (2019) found that a Mamawi Creek avulsion (also known as the "Cree Creek diversion," Prowse et al., 1996, or Embarras Breakthrough, Kay et al., 2019) that occurred in 1982 (Figures 1b and 1c) has increased inundation patterns along Mamawi Creek and decreased flooding along the lower Athabasca River sectors of the delta (Kay et al., 2019).

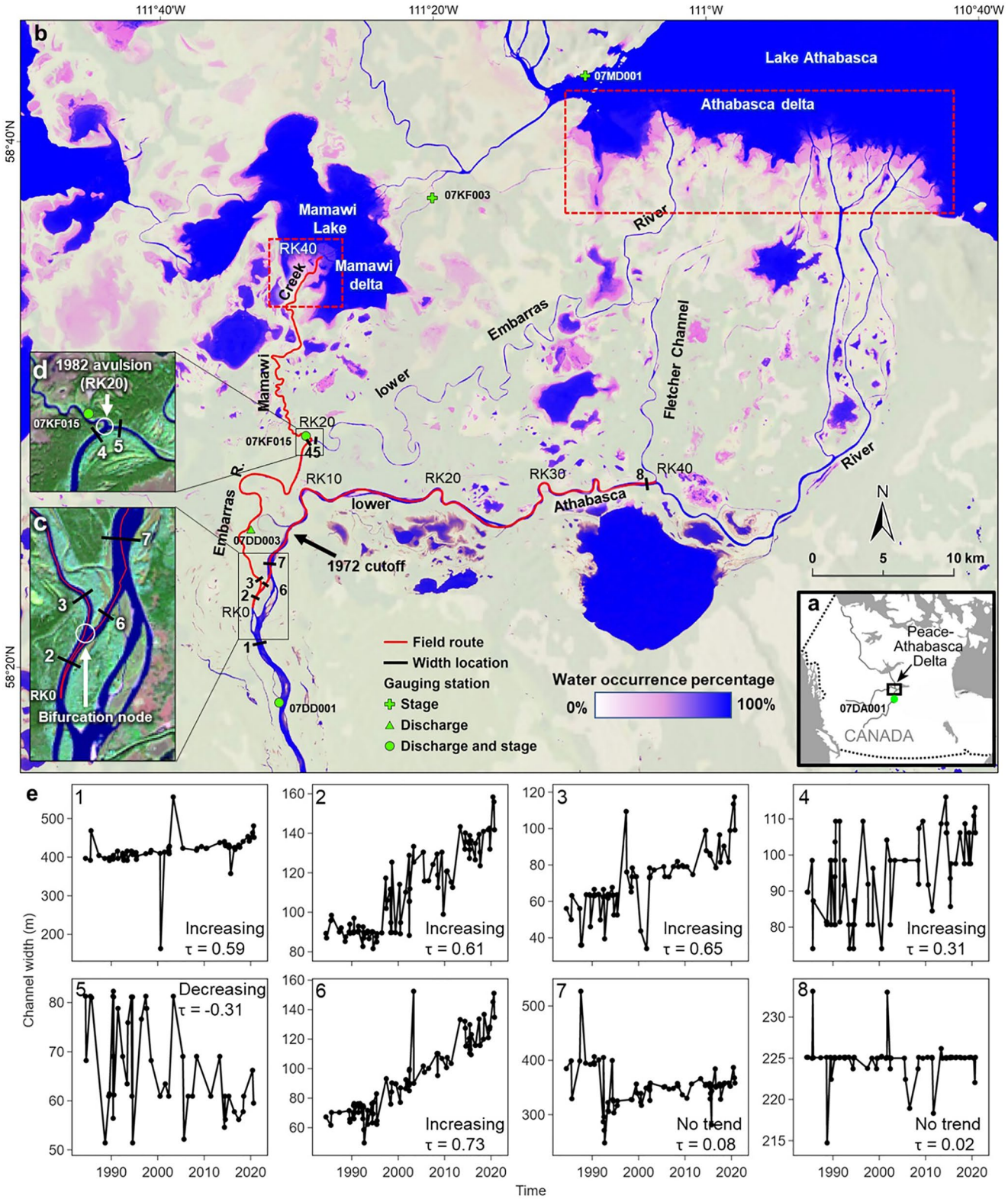
111°40'W
111°20'W
111°W
110°40'W
58°40'N
58°20'N
b
Lake Athabasca
07MD001
Athabasca delta
07KF003
Mamawi Lake
RK40
Creek
Mamawi delta
Embarras
River
Fletcher Channel
Mamawi
lower
RK20
07KF015
RK10
RK30
RK40
Athabasca
River
d 1982 avulsion (RK20)
07KF015
c
RK0
Bifurcation node
07DD003
1972 cutoff
07DD001
N
0 5 10 km
a
Peace-Athabasca Delta
07DA001
CANADA
Field route
Width location
Gauging station
Stage
Discharge
Discharge and stage
Water occurrence percentage
0%
100%
e
1 Increasing τ = 0.59
2 Increasing τ = 0.61
3 Increasing τ = 0.65
4 Increasing τ = 0.31
5 Decreasing τ = -0.31
6 Increasing τ = 0.73
7 No trend τ = 0.08
8 No trend τ = 0.02
Channel width (m)
Time
1990 2000 2010 2020

Figure 1.

Table 1
Environment and Climate Change Canada (ECCC) Gauging Stations Used in This Study

Station ID	Station name	Discharge	Stage
07DA001	Athabasca R. below Fort McMurray	1958-present	2012-present
07DD001	Athabasca R. at Embarras Airport	1971–1984, 2014-present	2014-present
07DD003	Athabasca R. below divergence	1987-present	–
07KF015	Embarras R. breakout to Mamawi Lake	1987-present	2015, 2017–2018
07KF003	Mamawi Lake Channel at Old Dog Camp	–	1971-present
07MD001	Lake Athabasca at Fort Chipewyan	–	1930-present

A 1970 field investigation discovered that the Athabasca River mainstem was at risk of avulsing into its adjacent major Embarras River distributary. By 1972, these two river channels were separated by only 50 m at the meander bend (see large oxbow NW of "1972 cutoff location" in Figure 1b). To prevent an Athabasca River avulsion, an artificial cutoff of the meander bend was completed in 1972 (Bayrock & Root, 1972, see also Figure 1b). Despite these engineering efforts, a partial avulsion of the Embarras River into Mamawi Creek occurred abruptly in 1982, diverting some Embarras water to Mamawi Lake through a newly formed crevasse (Figures 1b and 1c) that connected to an existing channel. The fraction of summertime Athabasca River mainstem flow diverted through this new EM pathway increased from 5% in 1987 to 15% by 2014 (K. Timoney & Lee, 2016), while the downstream Mamawi Creek delta prograded at a faster rate than Athabasca River delta (i.e., sediment-normalized areal growth of 0.63 vs. 0.22 $km^2\ Mt^{-1}$ between 1981 and 2014 (K. Timoney & Lee, 2016)). This small but growing flow path for Athabasca River water through the Embarras River and Mamawi Creek is thus a potential slow avulsion course for the Athabasca River mainstem, and we hereafter refer to it as "Embarras-Mamawi" or EM channel.

3. Data and Methods

In this study, we evaluate the EM channel as a potential avulsion course for the Athabasca River. Two ∼40 km channel reaches are selected for analysis, the EM and the lower Athabasca River (red lines in Figure 1b), both starting 1 km upstream of the Athabasca-Embarras bifurcation (RK0, Figures 1b and 1c). The downstream ends of these two ∼40 km courses are Mamawi Lake and Fletcher Channel inlet (indicated as "RK40" at two locations on the location map, Figure 1b), respectively. We assess the hydrological and geomorphological characteristics along these two courses using in situ and remotely sensed datasets, as described next.

3.1. Hydrological Measurements From Gauging Stations

Multiple river and lake gauges are located in the PAD, operated by the Water Survey of Canada, Environment and Climate Change Canada (ECCC) as part of the National Hydrometric Network. We obtain discharge and stage data for from six ECCC stations (Table 1 and Figure 1). Because the Athabasca River discharges at station 07DD001 (established in 1971) were not collected from 1984 to 2014 (Figure S1 in Supporting Information S1), we estimate missing data for 07DD001 using the station 07DA001, located ∼200 km upstream near Fort McMurray (Figure 1a). Lagged correlation analysis reveals a time lag of 2 days between the two stations (Figure S2 in Supporting Information S1). A linear regression model with these two stations based on 1971–1984 and 2014–2020, with 80% of overlapping data used for regression training and 20% for validation, was used

Figure 1. (a) The Peace-Athabasca River Delta (PAD) is located in northeastern Alberta, Canada. (b) The Embarras River is a distributary of the Athabasca River that flows east into Lake Athabasca, but has diverted a growing share of Athabasca mainstem discharge northward into Mamawi Lake following its partial avulsion into Mamawi Creek in 1982. This developing Embarras-Mamawi (EM) channel thus represents a potential slow avulsion course for the Athabasca River and is the focus of this study. Historical discharge and stage records are available from 6 Water Survey of Canada gauging stations (green symbols) distributed throughout the PAD and another ∼200 km upstream. Red lines indicate our two study reaches: the 40 km Embarras-Mamawi channel and a 40 km length of Athabasca River. Supplementary in situ measurements of discharge, water depth, and water surface elevation data along these two channels were collected in the summer 2018. (c) Enlarged view of the Athabasca-EM bifurcation node. (d) Enlarged view of the 1982 Mamawi Creek avulsion site. (e) Landsat-derived time series of channel width variations at eight locations along the two study reaches, together with Mann-Kendall trend test statistics (increasing, decreasing, or no trend). Mann-Kendall tau (τ) coefficient values greater (less) than +0.30 (−0.30) indicate significant positive (negative) trend. The numbers 1 through 8 in the graphs correspond to numbers found in the (b)–(d) panels.

to estimate missing data with a mean absolute error (MAE) of 59 $m^3\ s^{-1}$ ($R^2 = 0.97$) (Figure S3 in Supporting Information S1).

The observed/simulated discharge data on the lower Athabasca River (07DD001) were then used to analyze the flow ratios between Embarras River (07DD003) and Mamawi Creek (07KF015) during 1984–2021.1984 was chosen as the start year of our study as it corresponds to the availability of Landsat data. We divide this period into seven sub-periods determined by available remote sensing imagery (Section 3.3). ANOVA analysis (Table S2 in Supporting Information S1) is then used to test the significance level of discharge ratios between the Embarras River and the Athabasca River, during seven different subperiods (1984–1988, 1988–1993, 1993–1998, 1998–2002, 2002–2008, 2008–2015, 2015–2021). The 1984–1988 ratio is calculated based on 241 matching data pairs between 30 July 1987 and 3 August 1988 because there were no discharges available from Embarras River before 1987.

3.2. Time-Series of Channel Widths From Landsat Satellite Imagery

Channel width can be estimated from remote sensing imagery for channels that are at least ~2X wider than the pixel length dimension (Jensen, 2008). Traditionally, historical time series analysis of channel width changes was time-intensive due to the need to download and analyze Landsat images individually, but cloud computing now makes this task straightforward. Here, we use RivWidth Cloud, an algorithm implemented in Google Earth Engine, to automatically extract channel widths from remotely sensed time series (X. Yang et al., 2020). For a single Landsat image (Landsat 5, 7, and 8), RivWidth Cloud returns channel widths at the 30-m resolution, extracted along predetermined centerlines from the Global River Widths from Landsat (GRWL) data product (G. H. Allen & Pavelsky, 2018). Users may select points of interest along GRWL centerlines, and the algorithm automatically returns a time series of channel width estimates from all available Landsat images satisfying user-specified conditions, such as cloud coverage and time period.

In this study, we select eight locations along the two 40 km channels (labeled 1–8, Figure 1b). Channel width variations from 1984 to 2020 are calculated at these locations using RivWidth Cloud. All available Landsat images with a cloud cover of <10% are used to generate a time series of width variations. No location is selected along Mamawi Creek as its channel is too narrow for satisfactory width estimation using 30 m Landsat imagery. The non-parametric Mann–Kendall trend test (Kendall, 1975; Mann, 1945) is used to determine the presence or absence of a statistically significant trend in each of the 8 channel width time-series, with a Mann-Kendall tau (τ) coefficient value greater (less) than +0.30 (−0.3) indicating a significant positive (negative) trend based on our sample size.

3.3. Time-Series of Delta and Channel Bar Surface Areas From Landsat Imagery

Landsat images between 1984 and 2021 are used to estimate surface area changes of the Mamawi Creek and Athabasca River deltas, and of large channel bars found in two locations along the Athabasca River. The selection of Landsat images acquired during similar water levels (stage) is critical for such surface area estimates to be useful for long-term change detection. Therefore, we first match all available Landsat imagery to lake stage observations at 07MD001 (Lake Athabasca) and 07KF003 (Mamawi Lake), and river stage observations at 07DD011 (Athabasca River), respectively. Next, images with an approximate 5-yr sampling frequency and acquired only when stages were within 0.01 m of a fixed elevation (209.246, 209.182, and 212.000 m, for stations 07MD001, 07KF003, and 07DD011, respectively) are selected for quantification of surface area changes of these deltas and bars (Table 2). This process minimizes the effects of stage fluctuations on surface area estimation.

For each of the selected Landsat images, we calculate the Modified Normalized Difference Water Index (MNDWI, Xu, 2006) to distinguish land from water:

$$\mathrm{MNDWI} = \frac{\mathrm{Green} - \mathrm{SWIR}}{\mathrm{Green} + \mathrm{SWIR}} \quad (1)$$

For Landsat 5 and 7, Green and SWIR bands are bands 2 and 5. For Landsat 8, Green and SWIR are bands 3 and 6. Delta shorelines on 30 July 1984, are used as a baseline for the Athabasca and Mamawi deltas, with subsequent land surface area changes calculated from each MNDWI to create a time series of delta surface areas. These

Table 2
Selected Landsat Images Used to Estimate Surface Area Changes of the Athabasca River Delta, Mamawi Creek Delta, and Two Large Channel Bars in the Athabasca River

Location	Number	Date	Station ID	Stage (m)	Landsat_ID
Athabasca delta	1	7/30/1984	07MD001	209.25	LT05_043019_19840730
Athabasca delta	2	6/10/1989	07MD001	209.24	LT05_043019_19890610
Athabasca delta	3	6/8/1994	07MD001	209.28	LT05_043019_19940608
Athabasca delta	4	8/22/1998	07MD001	209.24	LT05_043019_19980822
Athabasca delta	5	8/5/2003	07MD001	209.33	LE07_042019_20030805
Athabasca delta	6	7/23/2007	07MD001	209.23	LT05_042019_20070723
Athabasca delta	7	7/28/2012	07MD001	209.27	LE07_042019_20120728
Athabasca delta	8	10/3/2019	07MD001	209.23	LC08_043019_20191003
Mamawi delta	1	7/30/1984	07KF003	209.18	LT05_043019_19840730
Mamawi delta	2	5/21/1990	07KF003	209.18	LT05_042019_19900521
Mamawi delta	3	6/8/1994	07KF003	209.23	LT05_043019_19940608
Mamawi delta	4	8/22/1998	07KF003	209.22	LT05_043019_19980822
Mamawi delta	5	8/5/2003	07KF003	209.27	LE07_042019_20030805
Mamawi delta	6	7/23/2007	07KF003	209.20	LT05_042019_20070723
Mamawi delta	7	7/28/2012	07KF003	209.21	LE07_042019_20120728
Mamawi delta	8	10/3/2019	07KF003	209.20	LC08_043019_20191003
Channel bars	1	7/30/1984	07DD011	212.08	LT05_043019_19840730
Channel bars	2	8/3/1988	07DD011	212.04	LT05_042019_19880803
Channel bars	3	5/29/1993	07DD011	212.13	LT05_042019_19930529
Channel bars	4	7/30/1998	07DD011	211.93	LT05_042019_19980730
Channel bars	5	6/14/2002	07DD011	211.93	LT05_043019_20020614
Channel bars	6	8/9/2008	07DD011	212.11	LE07_043019_20080809
Channel bars	7	5/26/2015	07DD011	211.99	LC08_042019_20150526
Channel bars	8	9/22/2021	07DD011	211.94	LC08_043019_20210922

Note. The images are selected during times of similar WSC gauge stages between acquisitions.

surface area time series are normalized by time (in years) and total flow volume (in km^3) for each subperiod using available discharge data (Table 1).

3.4. Longitudinal Depth and Water Surface Elevation Profiles From GNSS Surveys

From 3 to 25 August, 2018, we measured longitudinal profiles of WSE and channel depth along the two study channels (Figure S4 in Supporting Information S1). Measurements were collected by motorboat using a Septentrio PolaRX5 global navigation satellite systems (GNSS) receiver with a PolaNt-x MF antenna mounted on a 2 m pole, and a single-frequency (200 kHz) HydroLite-TM (Seafloor Systems) depth sounder. Since the GNSS receiver and depth sounder were left logging throughout the day, the draft or tilt of the boat could change as people or equipment moved within the vessel. To mitigate errors associated with such weight distribution changes, offsets from the water surface were measured against both the GNSS antenna and depth sounder transducer and used to correct the final data set. GNSS measurements were logged at 1 Hz sampling frequency and processed to 3D coordinates via Natural Resources Canada's Canadian Spatial Reference System Precise Point Positioning (CSRS-PPP) online tool (https://webapp.geod.nrcan.gc.ca/geod/tools-outils/ppp.php?locale=en), with typical 95% uncertainty bounds per measurement of 3 cm horizontally and 7 cm vertically. Depth measurements with a nominal accuracy of 0.1% were logged at a 2 Hz sampling frequency, averaged to 1 Hz, and then joined to the GNSS measurements based on timestamp. Measurements were excluded if they were equal to 0 or greater than 30 m, there were no concurrent GNSS measurements within 1 s, there was no depth sounder offset taken, or if the two 2 Hz measurements used for averaging differed by >8%. In sum, continuous longitudinal measurements of

WSE and channel depth were collected for ~80 km of the Athabasca River, Embarras River, and Mamawi Creek over the 21-day field campaign. A further ~100 km was collected at other locations and times on the PAD that are not utilized here.

We transform the datum of WSE and depth measurements from the default NAD83 to CGVD2013 Epoch2010 to match the reference system for ECCC stage data. The transformation is completed using a model published by Natural Resources Canada (https://webapp.geod.nrcan.gc.ca/geod/data-donnees/geoid.php?locale=en), which has a 3.7 km resolution in the study area. The elevation difference between the two datums is extracted from the geoid based on location and is then added to the NAD83 data to obtain CGVD2013 height.

To calculate WSS, we first manually digitize centerlines down the Athabasca River, Embarras River, and Mamawi Creek (red lines in Figure 1). These lines are close as possible to the channel centers and approximately coincide with our in situ GNSS profiles. Next, 30-m interval points along these lines are generated in ArcGIS Pro 2.7. For each point, we calculate the average WSE and standard deviation of the surrounding GNSS points within a user-specific search radius, using the spatial join function. To minimize the effects of riverbanks and trees on the GNSS signal, 100-m and 20-m search radii are used for the Athabasca River and the Embarras-Mamawi channel, respectively, due to their different channel widths. Average WSS is then calculated using a linear regression within a 5 km moving window along the Athabasca, Embarras, and Mamawi Creek centerlines.

3.5. Longitudinal Discharge Measurements From ADCP

Together with the WSE and depth measurements, river discharge was measured by ADCP every ~500–1,000 m along the studied river channels at 93 locations during August 2018 (Harlan et al., 2021). At least two discharge transects were collected at every location with a SonTek RiverSurveyor M9 ADCP mounted to the side of the motorboat. Stringent quality control criteria were used to exclude lower-quality measurements, including verifying that at least two discharge measurements per location agreed to within 5%, sufficiently slow boat speed, sampling covering at least 70% of each river cross-section, and others as described in Harlan et al. (2021).

3.6. Stream Power and Bed Shear Stress Calculations

Stream power is a useful tool to characterize potential sediment erosion, transport, and deposition through a channel (Bagnold, 1960, 1966; Gartner et al., 2015; Richards, 1982). To create longitudinal profiles of stream power along the Athabasca River and the Embarrass-Mamawi channel, we calculate it from our in situ measurements as (Bagnold, 1960, 1966):

$$\Omega = rqs \tag{2}$$

where Ω is the stream power per unit of flow length (W m^{-1}), r is the specific weight of water (9,800 N m^{-3}), q is the discharge (m^3 s^{-1}) from Harlan et al. (2021), and s is the WSS (m m^{-1}) from our GNSS measurements (see Section 3.4). Unit stream power (ω), which is strongly correlated to total bed-material load (C. T. Yang, 1979), was computed based on channel width (b) as measured in the field by Harlan et al. (2021):

$$\omega = \frac{rqs}{b} \tag{3}$$

Bed shear stress of the flow acting on the bed material is frequently employed as a measure of a stream's ability to entrain bed material:

$$\tau = rRs \tag{4}$$

where τ is the bed shear stress and R is the hydraulic radius, here approximated as mean water depth (Babaeyan-Koopaei et al., 2002) across the ADCP cross-section.

4. Results

4.1. Discharge Analysis of the Athabasca River and Embarras-Mamawi Channel

Comparison of discharge records show that the fraction of Athabasca River water entering the Embarras River increased notably from 1987 to 2021 (Figure 2). The average discharge in the Athabasca River (07DD001) increased from 634 m^3 s^{-1} during 1984–1988 to 765 m^3 s^{-1} during 2015–2021 (Table 3). The average discharge in

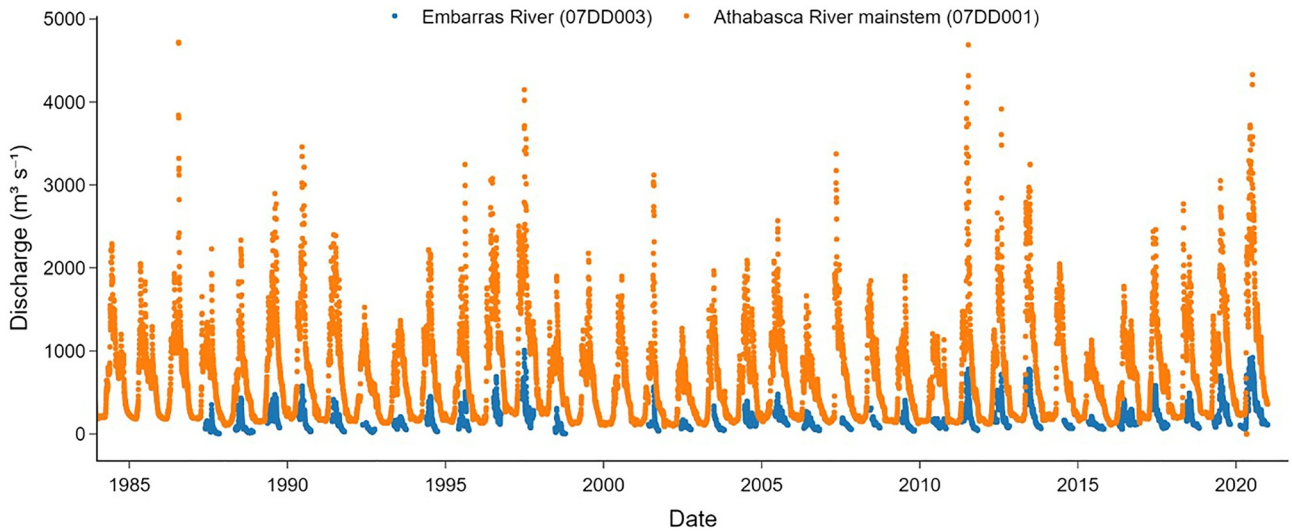

Figure 2. Daily discharges in the Athabasca River upstream of the Athabasca-Embarras bifurcation (Environment and Climate Change Canada gauging station 07DD001, orange line) and in the Embarras River (07DD003, blue line) from 1984 to 2021. The Embarras River at 07DD003 has no data before 1987.

the Embarras River (07DD003) increased from 102 $m^3\ s^{-1}$ during 1984–1988 to 224 $m^3\ s^{-1}$ during 2015–2021 (Table 3). Therefore, although discharge increased ~20% in the Athabasca River, the amount of water entering the Embarras River more than doubled. The discharge ratio between the Embarras and Athabasca Rivers increased from 9% during 1984–1988 to 21% during 2015–2021 over seven different periods between 1984 and 2021 (Figure 3 & Table 3). The only exception is the period 1998–2002, but this exception may be an artifact of missing discharge data during this time (i.e., only 145 observations during 1998–2002 vs. 241–1,196 observations during other periods).

The fraction of Embarras River discharge entering Mamawi Creek also increased from 1984 to 2021. The average discharge at Mamawi Creek (07KF015) more than doubled from 59 $m^3\ s^{-1}$ during 1984–1988 to 128 $m^3\ s^{-1}$ during 2015–2021 (Table 4). Accordingly, the discharge ratio between Mamawi Creek and Embarras River increased from 64% to 68% between 1984 and 2021. The discharge ratio between the Mamawi Creek and the much larger Athabasca main channel (07DD001) increased from 5% to 12% during the same period (Table 4). Therefore, relative to the Athabasca River, the discharge increase in Embarras River and Mamawi Creek has a similar rate (both doubled).

4.2. Channel Width Variations Along the Athabasca River and the Embarras-Mamawi Channel

Time-series analysis of remotely sensed channel widths from 1984 to 2020 reveals that the Embarras River has gradually widened upstream of the Embarras-Mamawi bifurcation (1982 avulsion site) but has narrowed

Table 3
Descriptive Statistics of Athabasca River (Environment and Climate Change Canada Station 07DD001) and Embarras River (07DD003) Discharges During Seven Different Time Periods Between 1984 and 2021

		Embarras ($m^3\ s^{-1}$)				Athabasca ($m^3\ s^{-1}$)				Ratio (Embarras/Athabasca)			
Period	Count	Mean	Std	Min	Max	Mean	Std	Min	Max	Mean	Std	Min	Max
1984–1988	241	103	98	4	433	634	508	104	4,720	0.09	0.05	0.01	0.21
1988–1993	616	137	114	14	579	637	565	134	3,458	0.11	0.04	0.04	0.22
1993–1998	606	209	160	20	1,010	765	635	135	4,148	0.15	0.05	0.02	0.38
1998–2002	145	95	117	4	566	450	422	90	3,119	0.10	0.06	0.01	0.20
2002–2008	840	135	73	44	479	596	476	107	3,373	0.16	0.03	0.10	0.32
2008–2015	968	191	155	36	782	608	597	122	4,689	0.18	0.03	0.12	0.29
2015–2021	1,196	226	170	57	923	765	644	110	4,330	0.21	0.05	0.13	0.45

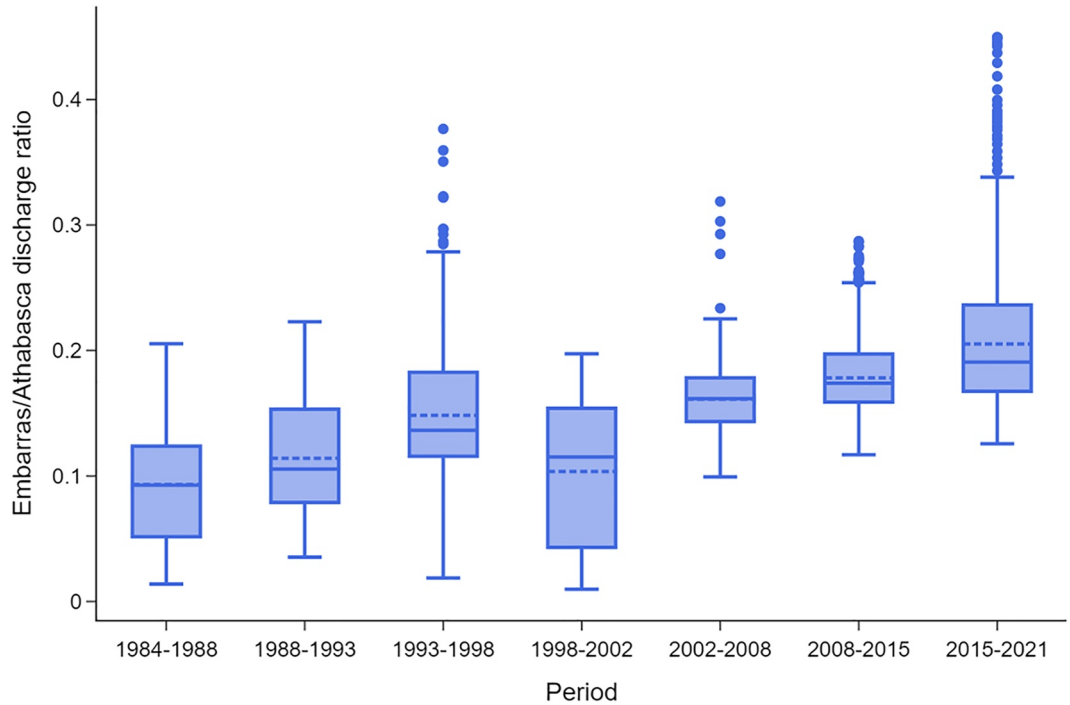

Figure 3. Boxplot of discharge ratio between the Embarras River (07DD003) and the Athabasca River (07DD001) during seven different periods between 1984 and 2021. Periods of 1984–1988 and 1998–2002 only have partial data (Figure 2).

downstream of the bifurcation (Figure 1e; Table 5). From 1984 to 2020, the Embarras River channel upstream of Mamawi Creek widened by +43 m (+85%) at location 3 and + 18 m (+21%) at location 4. Downstream of Mamawi Creek, the lower Embarras River at location 5 narrowed by 60 m (−12%) from 1984 to 2020. All of these width trends are statistically significant (Mann Kendall τ = 0.65, 0.31, 0.31 for locations 3, 4, and 5, respectively). While the Mamawi Creek channel is too narrow to be accurately measured from 30-m Landsat imagery, the observed widening/narrowing trends upstream/downstream of its bifurcation from the Embarras strongly suggest its enlargement.

In contrast to the Embarras River, the lower Athabasca River (downstream of the Athabasca-bifurcation) shows little change in channel width, narrowing by −43 m (−11%) at location 7 and no change at location 8 (Figure 1 and Table 5). No statistically significant trends are found at these locations (Mann Kendall τ = 0.08, 0.02, respectively).

Table 4
Mean Discharge and Discharge Ratios in the Athabasca River (07DD001), Embarras River (07DD003), and Mamawi Creek (07KF015) During Seven Different Time Periods Between 1984 and 2021

	Mean discharge ($m^3 s^{-1}$)			Mean discharge ratio		
Period	Athabasca	Embarras	Mamawi	Embarras/Athabasca	Mamawi/Athabasca	Mamawi/Embarras
1984–1988	634	103	59	0.09	0.05	0.64
1988–1993	637	137	80	0.11	0.07	0.66
1993–1998	765	209	121	0.15	0.09	0.65
1998–2002	450	95	88	0.10	0.10	1.78[a]
2002–2008	596	136	94	0.16	0.10	0.65
2008–2015	608	191	119	0.18	0.12	0.68
2015–2021	765	226	128	0.21	0.12	0.68

[a]Environment and Climate Change Canada reported only 145 discharge measurements during 1998–2002 for the Embarras River, which may impact this discharge ratio.

Table 5
Channel Width Analysis From Landsat Images and RivWidth Cloud

River	Location	#Images	Mean width 1984–1989 (m)	Mean width 2016–2020 (m)	Width change (m)	Change rate (%)	Mann Kendall
Athabasca	1	67	407	442	+35	+9	Increasing ($\tau = 0.59$)
Bifurcation	2	60	91	139	+48	+53	Increasing ($\tau = 0.61$)
Embarras	3	73	52	95	+43	+85	Increasing ($\tau = 0.65$)
Embarras	4	64	86	104	+18	+21	Increasing ($\tau = 0.31$)
Embarras	5	49	68	60	−8	−12	Decreasing ($\tau = 0.31$)
Bifurcation	6	85	67	128	61	+91	Increasing ($\tau = 0.73$)
Athabasca	7	86	404	358	−46	−11	No trend ($\tau = 0.08$)
Athabasca	8	93	225	225	0	0	No trend ($\tau = 0.02$)

Note. The Mann-Kendall test is used to establish statistical significance ($\tau > +0.3$ or $\tau < -0.3$) for all available Landsat-derived widths between 1984 and 2020 (#images). Mean widths are computed for the first (1984–1989) and last (2016–2020) 5 years of the satellite record.

Approximately 4 km upstream of the Embarras bifurcation, the Athabasca River widened slightly at location 1 (+35 m, or +9%) from 1984 to 2020 (statistically significant, $\tau = 0.59$). Immediately upstream and downstream of the bifurcation, a left channel of the Athabasca widened by +48 m (+53%) and +61 m (+91%) at locations 2 and 6, respectively (statistically significant, $\tau = 0.61$, 0.73, respectively). Such dramatic widening suggests that this left channel is becoming a dominant path for water and sediment transport immediately upstream of its partial diversion into the EM channel (Figure 1d).

4.3. Changes in Surface Area of Deltas, Channel Bars, and Floodplain Inundation

The Mamawi Creek delta is growing faster (proportionally) than the Athabasca River delta, suggesting a higher (discharge-normalized) sediment transport rate (Figure 4). Since 1984, a bird's foot delta at the Embarras-Mamawi channel mouth has rapidly prograded into Mamawi Lake (Figure 5). The delta's surface area growth averaged +2,810 m^2 per cubic kilometer of annual discharge ($m^2\ km^{-3}\ yr^{-1}$) between 1984 and 1998. Over the same period, the Athabasca River delta experienced a surface area loss averaging −890 $m^2\ km^{-3}\ yr^{-1}$ (Figure 6). After that, both deltas briefly expanded at a comparable rate (i.e., 97,884 vs. 92,139 $m^2\ km^{-3}\ yr^{-1}$) between 1998 and 2003 (Figures 4–6). After 2003, the Athabasca delta growth rate stabilized, averaging 10,145 $m^2\ km^{-3}\ yr^{-1}$ over the three periods between 2003 and 2019 (Figure 4). However, the Mamawi delta growth rate steadily increased

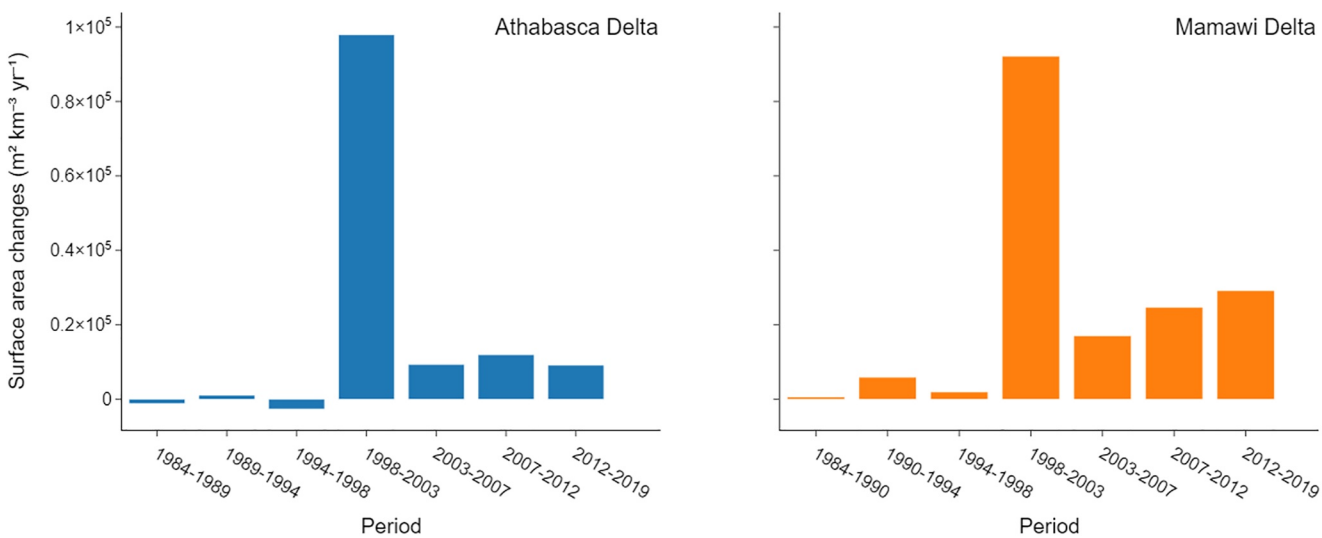

Figure 4. Discharge-normalized surface area change rate ($m^2\ km^{-3}\ yr^{-1}$) of the Athabasca River delta (left) and Mamawi Creek delta (right) during seven time periods between 1984 and 2019. Areal changes are mapped from Landsat imagery; discharges are from Environment and Climate Change Canada gauging stations (07KF003 and 07MD001).

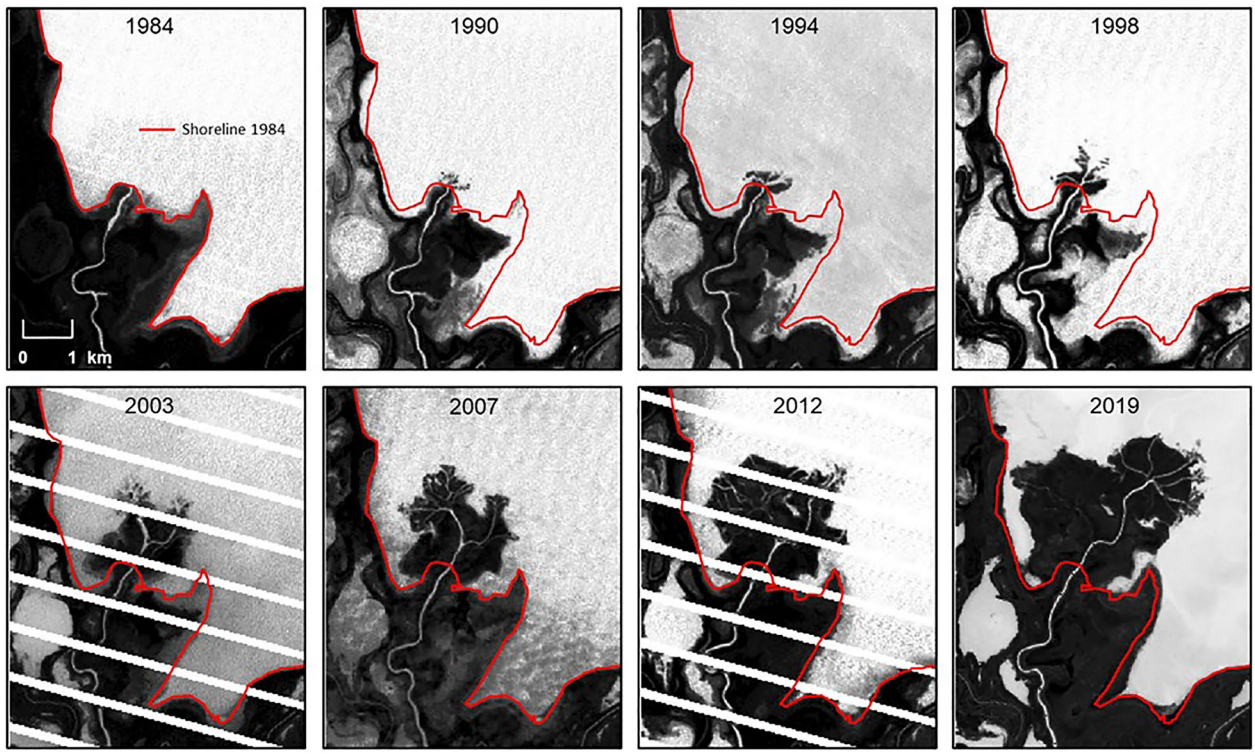

Figure 5. Growth of the Mamawi Creek delta as tracked by Landsat imagery between 1984 and 2019. Dark tones indicate land and light tones indicate water in these Modified Normalized Difference Water Index images. Landsat images were selected to be cloud-free and at the same Mamawi Lake stage (Environment and Climate Change Canada station 07KF003, Table 2, generally within ±5 cm).

with an average rate of 23,623 m^2 km^{-3} yr^{-1}. Aside from a brief period of rapid, commensurate growth from 1998 to 2003, these discharge-normalized delta growth rates suggest increasing sediment transport through the Embarras-Mamawi channel.

Channel bars grew significantly in two areas of the Athabasca River mainstem during our study period (Figure 7 and Figure S5 in Supporting Information S1). In 1984, a dominant right-bank Athabasca channel near the Embarras bifurcation contained several small bars with a combined surface area of 0.6 km^2 (Area 1, Figure 7; Table S1 in Supporting Information S1). By 2021, the combined surface area of these bars had grown to 1.3 km^2. Our own 2018 discharge measurements in this area (Harlan et al., 2021) documented ~60% of Athabasca River discharge flowing through the left-bank channel at that time (i.e., 578 m^3/s out of 993 m^3/s total, recorded 13 August 2018). The observed geometry of channel bar growth suggests that a channel switch is underway, with the left channel now conveying more discharge than the right. Some 13 km downstream, two large bars have also been developing (Area 2, Figure 7). Their combined surface area increased from 0.2 km^2 in 1984 to 0.6 km^2 in 2021, suggesting sediment deposition in the lower Athabasca River below the Embarras bifurcation.

As a consequence of the increasing diversion of Athabasca River flow into the Embarras-Mamawi channel, there are significant changes in downstream inundation patterns on the PAD. The Landsat-based global water occurrence change product of Pekel et al. (2016) reveals higher inundation frequency along the EM in 2000–2020 versus 1984–1999 (Figures 8a and 8b). In contrast, the lower Embarras River (downstream of the Embarras-Mamawi bifurcation) exhibits a narrowing channel and decreased inundation frequency (Figure 8c), and several large lakes have desiccated (Figure 8d). Similar drying is observed along the lower Athabasca River (Figure 8e). We also note significant drying nearer the Peace River northwest of Mamawi Lake, where several perched basins that were inundated in 1984–1999 were dry in 2000–2020 (Figure 8f).

4.4. Longitudinal Profiles of WSE, WSS, Discharge, and Water Depth

GNSS profiles of WSE show that downstream of the Athabasca-Embarras bifurcation, the Embarras-Mamawi channel (EM) has a much steeper WSS (8×10^{-5}) than the Athabasca River when measured in 2018 (4×10^{-5},

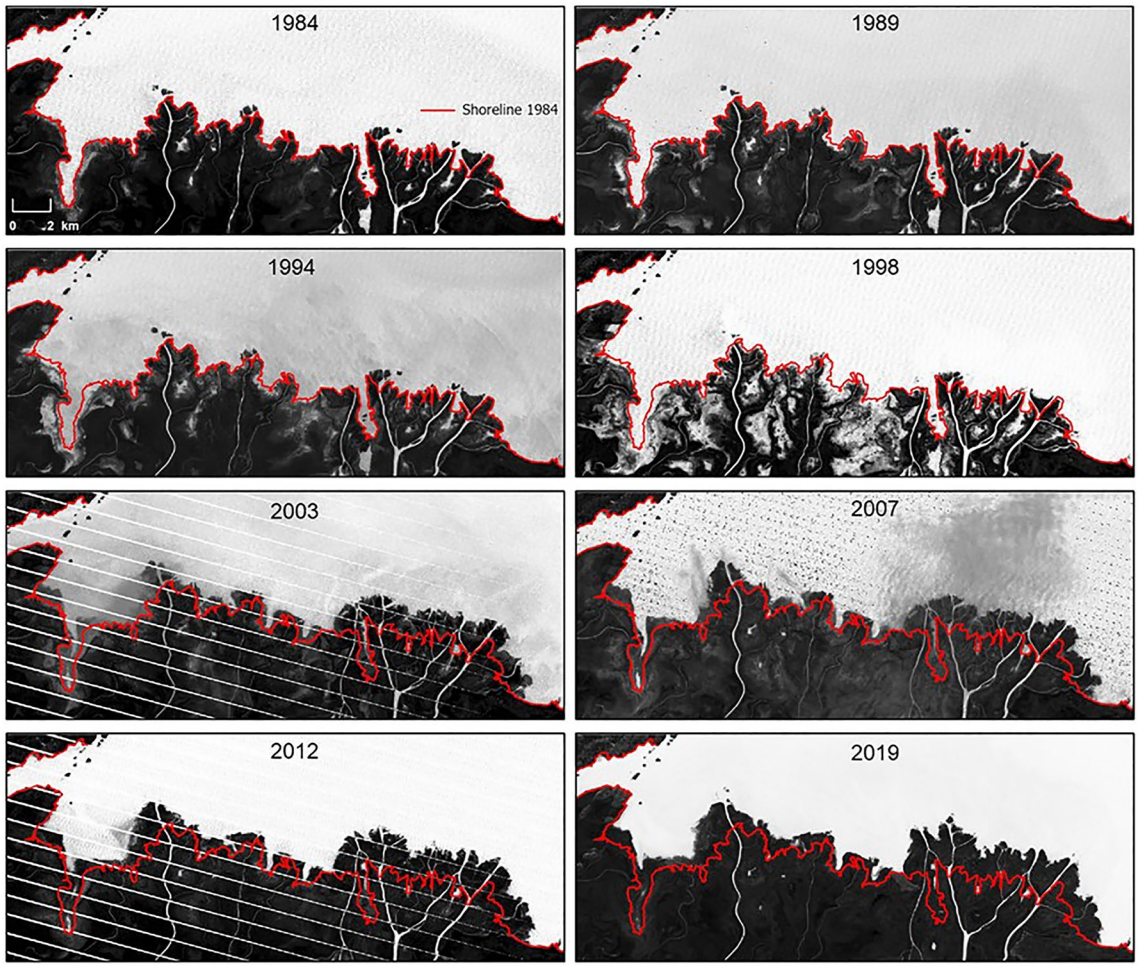

Figure 6. Surface area changes of the Athabasca River delta as tracked by Landsat imagery between 1984 and 2019. Dark tones indicate land and light tones indicate water in these Modified Normalized Difference Water Index images. Landsat images were selected to be cloud-free and at the same Lake Athabasca stage (Environment and Climate Change Canada station 07MD001, Table 2, generally within ±5 cm).

Figure 9). A locally weighted regression line indicates that the EM has relatively uniform WSS through the 40 km channel, while the Athabasca River has varying WSS. The latter exhibits a gentler slope in the first 13 km and the last 10 km reach prior to its bifurcation at Fletcher Channel (Figure 9).

During the 2018 ADCP measurements, the average discharge was 937, 214, and 144 $m^3\ s^{-1}$ for the Athabasca River, Embarras River, and Mamawi Creek, respectively. The discharge ratios of Embarras/Athabasca and Mamawi/Embarras were 23% and 67%, respectively. These 2018 ratios are consistent with our calculated average discharge ratio for 2015–2021 using ECCC gauging station data (Tables 3 and 4).

Average water depths collected during the 2018 field campaigns were 4.6 and 1.6 m for the Athabasca River and the EM, respectively (Figure 10). Average EM water depth is 2.2 m upstream of the Embarras-Mamawi bifurcation and drops to 1.3 m in Mamawi Creek. Despite noisy data in both channels caused by the boat not always passing over the thalwegs, depth variation is much larger in the wider Athabasca River due to apparent crossings and pools. Bed elevation differences also exist between bifurcated and main channels. At the Athabasca-Embarras bifurcation, the bed elevation in the Embarras River is 0.6 m higher than the Athabasca River. At the Embarras-Mamawi bifurcation, the bed elevation in the Mamawi Creek is about 2.5 m higher than the Embarras River.

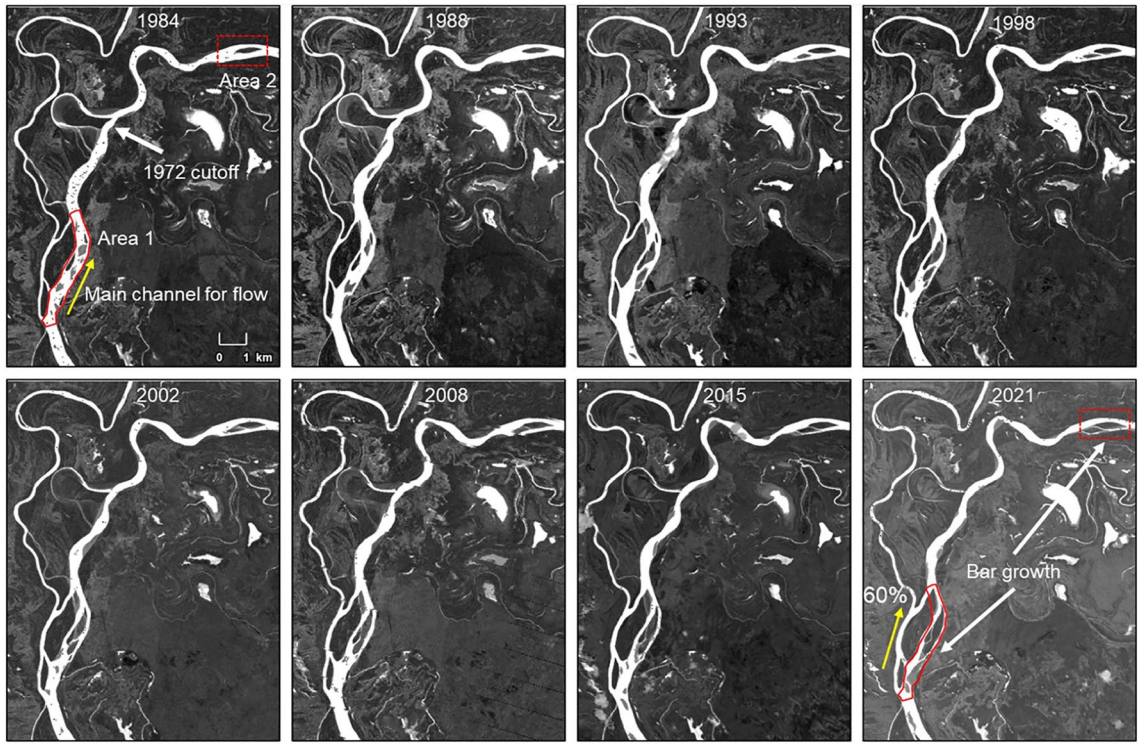

Figure 7. Growth of Athabasca River channel bars between 1984 and 2021 as reconstructed from Landsat satellite images. Dark tones indicate land and light tones indicate water in these Modified Normalized Difference Water Index images. Landsat images were selected to be cloud-free and at the same Athabasca River stage (Environment and Climate Change Canada station 07DD011, Table 2, generally within ±5 cm). In 1984, the right channel near the Athabasca-Embarras bifurcation was dominant (Area 1). By 2018 the left channel was dominant, carrying ~60% of Athabasca River discharge according to our field measurements. By 2021 the left channel is visibly dominant in Landsat imagery. The oxbow lake after the 1972 cutoff was relatively wide in 1984 but shrunk over time.

4.5. Longitudinal Profiles of Unit Stream Power and Bed Shear Stress

Calculations of unit stream power (ω) from in situ WSS and discharge measurements reveal broadly similar values, averaging ~2.0 and 1.7 W m^{-2} for the Athabasca and the Embarras-Mamawi channel, respectively. However, EM ω is highest below the Mamawi Creek bifurcation, whereas Athabasca River ω peaks far downstream of the potential avulsion course (Figure 11). Athabasca River ω declines sharply when the river approaches Fletcher Channel (~RK 32), owing mainly to reduced WSS (Figure 9). Along the EM, ω briefly dips in the Embarras (~RK12–RK19) but then increases ~19% downstream of the Embarras-Mamawi bifurcation, suggesting enhanced erosion potential along Mamawi Creek.

In terms of bed shear stress τ, the Athabasca River and the EM exhibit approximately similar values (τ = ~1.5) upstream of the Embarras-Mamawi bifurcation, but increase in Mamawi Creek downstream of the bifurcation (mean τ ~ 2.9), suggesting a greater ability to transport bedload (Figure 12). In contrast, mean bed shear stress decreases significantly in the Athabasca River downstream of RK 30, indicating greater deposition and less erosion approaching Fletcher Channel (Figure 12).

5. Discussion and Conclusion

The EM flow course appears to be a developing avulsion of the Athabasca River. Its gradual enlargement since 1982 is evident from multiple lines of observation including ECCC gauging stations, satellite images, and in situ field measurements. First, between 1984 and 2021 the discharge ratio between the Embarras-Mamawi channel and the Athabasca River more than doubled, increasing from 9% to 21%. Second, the Embarras-Mamawi channel has been widening since 1984, whereas the Athabasca River channel width has remained stable. Third, the Mamawi Creek delta is growing at a faster rate than the Athabasca River delta. Fourth, our longitudinal field GNSS surveys reveal that the Embarras-Mamawi channel possesses a significant slope advantage over

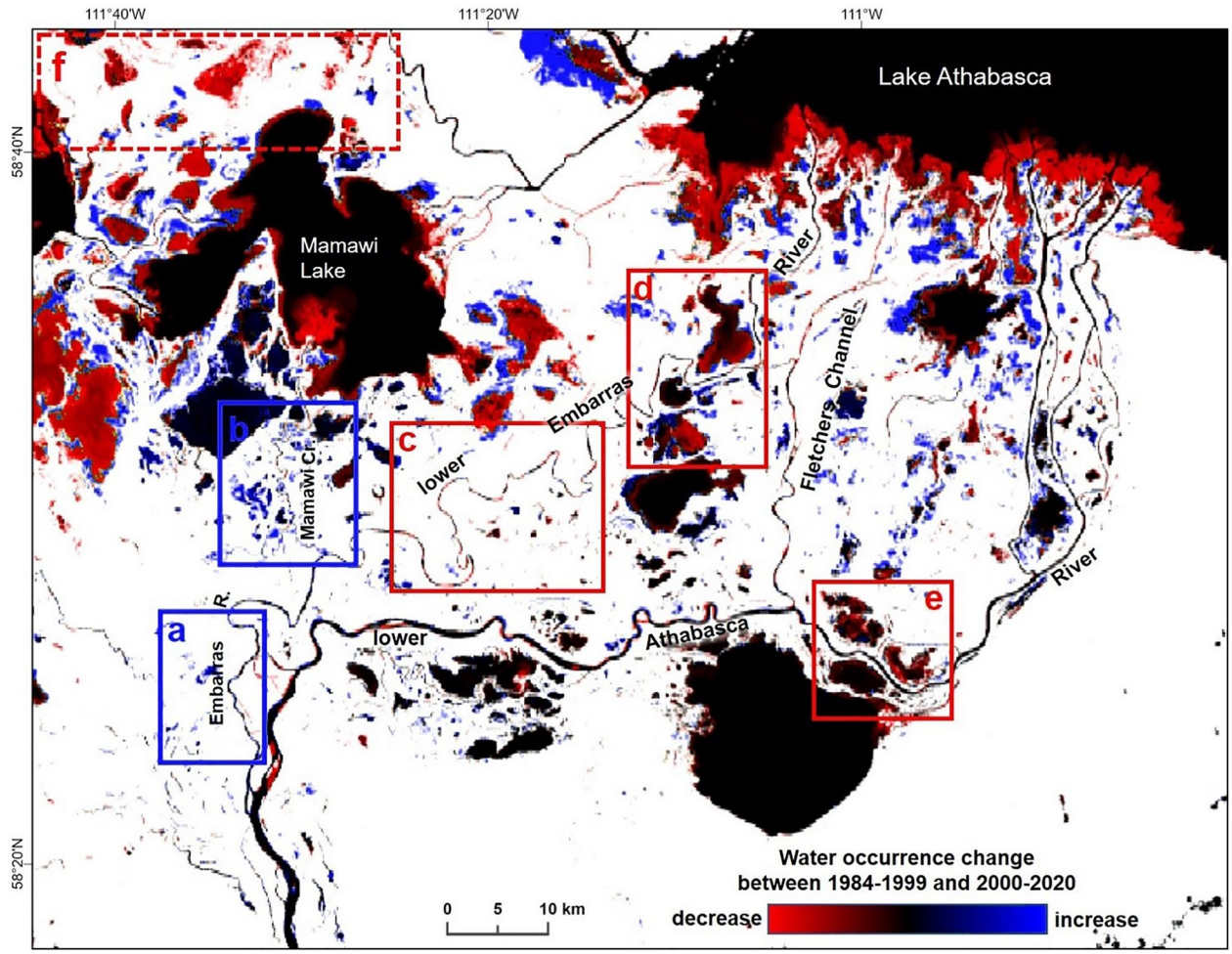

Figure 8. Landsat-derived water occurrence change frequency (Pekel et al., 2016) reveals both increased and decreased inundation across the Peace-Athabasca River Delta. Blue (red) colors indicate increased (decreased) water occurrence frequency between 1984–1999 and 2000–2020. Black tones indicate no change in water occurrence frequency. Increasing inundation is observed along the Athabasca-EM avulsion course (blue boxes a and b), with decreasing water occurrence downstream of Embarras-Mamawi bifurcation (red boxes c and d) and lower Athabasca River (box e). Significant drying is also noted in perched lake basins near the Peace River (red box f).

the Athabasca River. Finally, unit stream power and bed shear stress suggest enhanced sediment transport and erosional capacity through the Embarras-Mamawi channel.

The ongoing slow Athabasca River avulsion was initiated by the abrupt 1982 avulsion of the Embarras River into Cree Creek, a tributary of Mamawi Creek, which opened the Embarras River–Mamawi flow course with a higher WSS than the main Athabasca River. The potentially transformative impact that this avulsion pathway presents to the PAD's hydrology has been recognized since at least the 1970s (Appended correspondence, Bayrock & Root, 1972). Jones and Schumm (1999) attributed reasons of increases potential avulsion course slope (S_a) to natural levee/alluvial ridge growth, alluvial fan and delta growth (convexity), and tectonism (resulting in lateral tilting). Our study finds an additional process, by demonstrating that an abrupt avulsion in a river's distal distributary can also trigger a mainstem avulsion due to the opening of a new flow path having an overall higher slope.

This slow avulsion appears to be triggering some broader inundation pattern changes on the PAD. Previous studies have focused primarily on impacts of declining ice-jam floods on the lower Peace River (Beltaos, Prowse, & Carter, 2006; Prowse & Conly, 1998; Prowse & Lalonde, 1996; D. G. Smith, 2003; Toyra et al., 2002; Wolfe et al., 2006), an important cause of drying in the Peace Delta since the 1970s and a phenomenon we observe as well (see Figure 8f). However, in addition to this well-known change, we observe that the ongoing Embarras-Mamawi avulsion is directing increasing fluxes of Athabasca River water and sediment northwards toward Mamawi Lake.

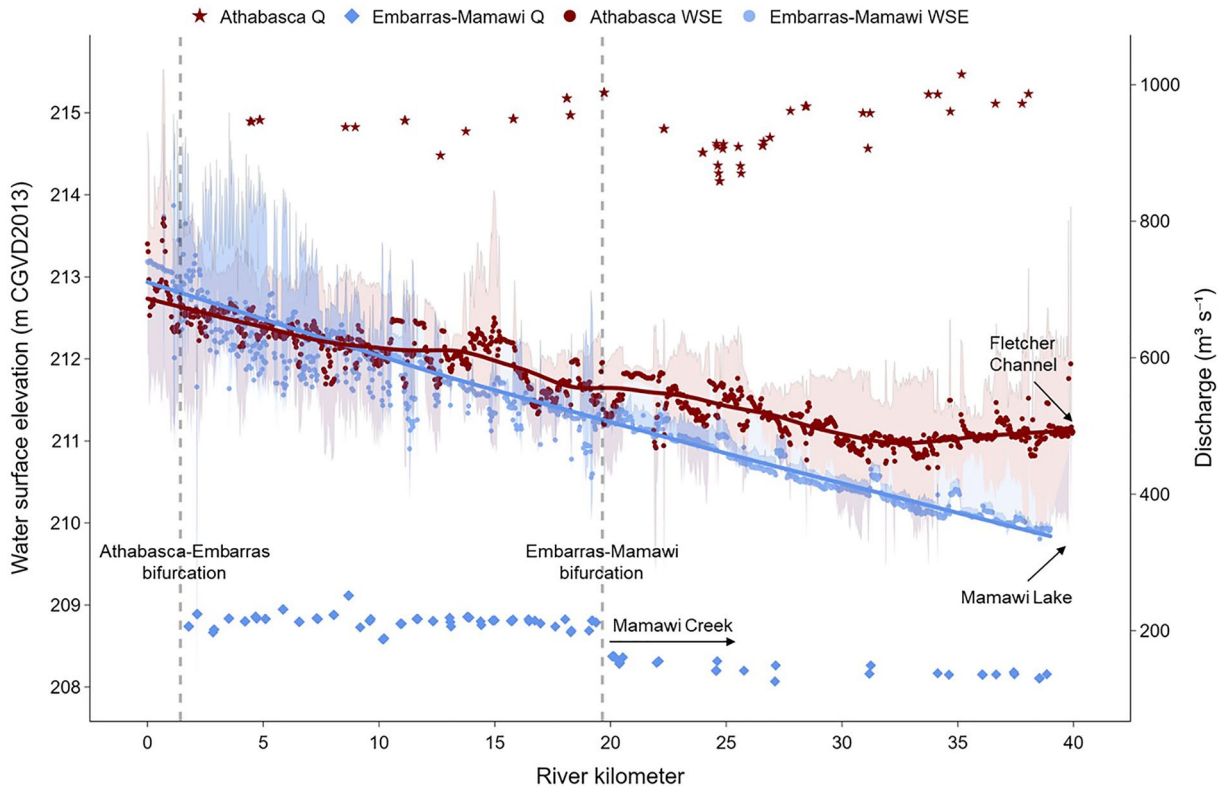

Figure 9. Longitudinal profiles of water surface elevation (WSE) and discharge (Q) collected 5–13 August, 2018 along the Athabasca River and the Embarras-Mamawi channel downstream of the Athabasca-Embarras bifurcation. Regression lines are from locally weighted scatterplot smoothing (LOWESS). Uncertainty bounds (shaded envelopes) represent the standard deviation for each averaged WSE measurement.

This finding is consistent with a paleohydrology study by Kay et al. (2019), who report increased flooding along Mamawi Creek but reduced flooding along the lower Athabasca River and attribute these changes to the 1982 Mamawi Creek avulsion. Our results support their conclusion and furthermore suggest that in addition to Mamawi Creek (Figure 8b), wetlands surrounding the upper Embarras River (Figure 8a) are receiving more water as well. Conversely, wetlands along the lower Embarras River (downstream of the Mamawi Creek bifurcation) are drying, likely due to diverted discharge (Figures 8c and 8d). Viewed collectively, these observations suggest that in addition to the impacts of reduced ice-jam flooding in the northern PAD (Figure 8f), inundation patterns in the southern PAD are also changing in areas not typically impacted by ice-jam floods (Figure 8). We attribute these changes in the southern PAD to increased diversion of Athabasca River water and sediment northward down the Embarras-Mamawi avulsion course.

Like K. Timoney and Lee (2016), we find that remote sensing of historical delta surface areas offers a useful tool for comparing relative sediment transport rates of neighboring channels. We build upon the approach of K. Timoney and Lee (2016) by processing more images in a cloud computing environment (Google Earth Engine), restricting satellite image selections to times of similar lake/river stage (to minimize the impact of fluctuating water levels on surface area determination), and using shorter sub study periods. Our 4–7-yr sampling frequency helps to pinpoint 1998–2003, for example, as a period when both the Athabasca and Mamawi deltas expanded rapidly (identified as 1992–2002 by K. Timoney & Lee, 2016). Both studies find faster relative growth of the Mamawi delta, suggesting higher sediment transport efficiency down the Embarras-Mamawi channel. Importantly, our study finds continued Mamawi delta growth during three consecutive periods after 2003, unlike the Athabasca delta (Figure 4). This recent deltaic growth averages ~0.71 km^2 yr^{-1} which if continued at this rate suggests that Mamawi Lake (91 km^2) would infill in ~130 years (Figure S9 in Supporting Information S1).

It is plausible that this current slow Athabasca River avulsion may accelerate in the future. Although a recent study by Peters et al. (2022) found a significant decline in March to October mean flows on the lower Athabasca River over the 1958 to 2017 period, Eum et al. (2017) projected an increase in mean annual and peak flows in the

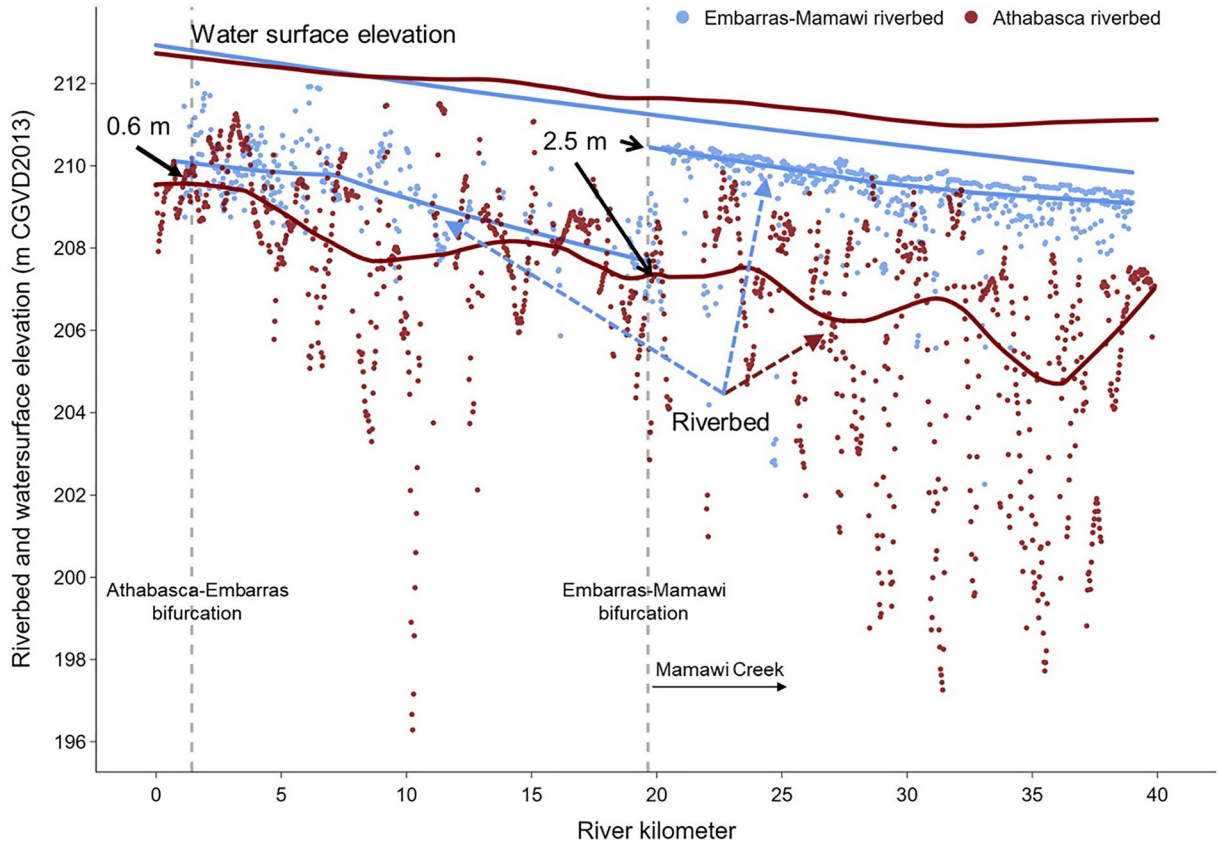

Figure 10. Longitudinal water surface elevation and riverbed elevation along the Athabasca River and the Embarras-Mamawi channel downstream of the two rivers' bifurcations. Regression lines are locally weighted scatterplot smoothing lines (LOWESS). At the Athabasca-Embarras bifurcation, the Embarras riverbed is ~0.6 m higher than the Athabasca riverbed. At the Embarras-Mamawi bifurcation, the Mamawi Creek bed is ~2.5 m higher than the Embarras riverbed.

second half of the 21st century. In response to projected changes in discharge, Dibike et al. (2018) estimated that $a > 50\%$ increase by the 2080s in the mean annual Athabasca River sediment load delivered to the PAD compared with sediment load in the 1980s. Elsewhere, modeling studies show that increased sediment transport can result in more avulsions and frequent switching of dominant channels (Bryant et al., 1995; Lauzon & Murray, 2022). Now originating on an outer bend of the Athabasca (Figure 1), the Embarras River receives water with somewhat lower bed materials and suspended sediment concentration (SSC) (e.g., 87 and 102 mg L^{-1} for the Embarras River and the Athabasca River, respectively; Pavelsky & Smith, 2009). This is because the higher riverbed in the Embarras River (i.e., 0.6 m higher, Figure 10) restricts bed material intaking from the main Athabasca River. Such disproportional water-sediment partitioning at avulsion bifurcations is similarly reported in modeling studies (Kleinhans et al., 2008; Slingerland & Smith, 1998). Increased sediment load could thus lead to enhanced sediment deposition and bar growth within the lower Athabasca River channels, further reducing WSS (i.e., reduced S_e, Jones & Schumm, 1999) and enhancing flow diversion northward through the Embarras-Mamawi channel toward Mamawi Lake.

At the turn of the last century, K. Timoney (2002) found that the PAD showed more signs of ecosystem health than problems by scoring of 26 physical and ecological attributes (e.g., flooding frequency, wetland productivity, open water area, etc.). Continued enlargement of the Embarras-Mamawi channel, however, could plausibly lead to full avulsion of the Athabasca River, a transformative impact that was likely narrowly averted in 1972 through human intervention. Throughout the Holocene, such major lobe-switching events have been a rare but normal process in PAD evolution (D. G. Smith, 1994), and indeed most other major deltas of the world (Bentley et al., 2016; Correggiari et al., 2005; Fisk, 1944; N. D. Smith et al., 1989; Vespremeanu-Stroe et al., 2017; Xue, 1993). A full Athabasca River avulsion into the Embarras-Mamawi channel, may lead to increasing wetland inundation around the new course, rapid sedimentary infilling of Mamawi Lake, and possibly more drying along

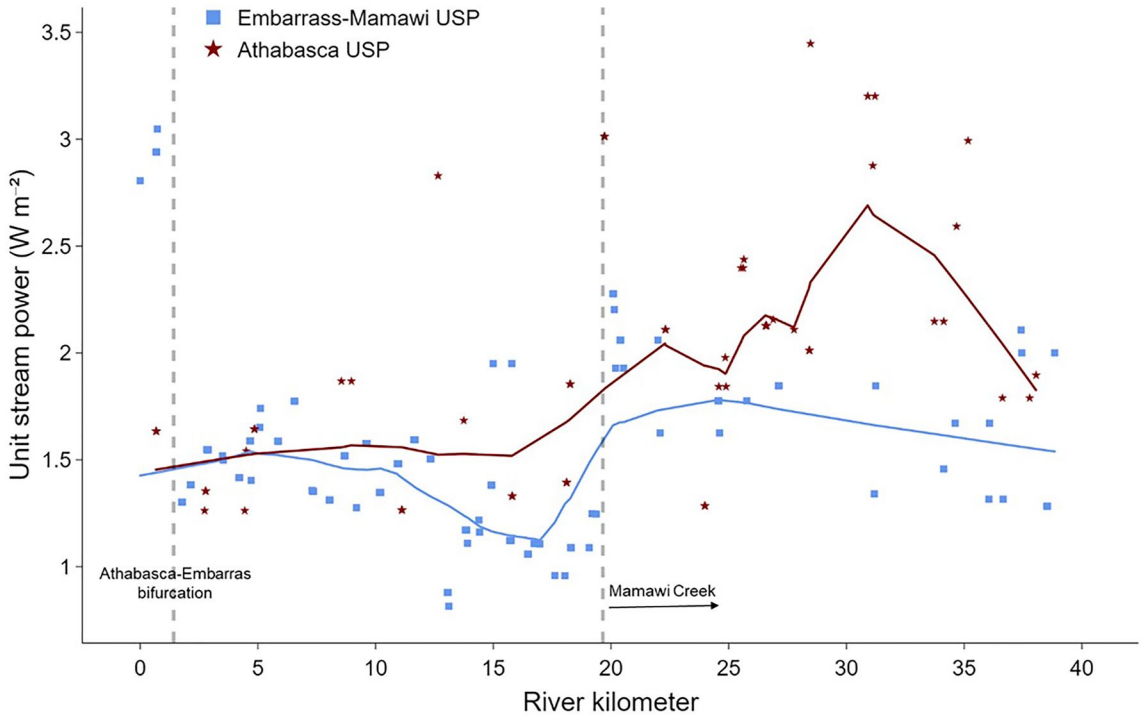

Figure 11. Longitudinal profiles of unit stream power (ω) along the Athabasca River and the Embarras-Mamawi channel downstream of the Athabasca-Embarras bifurcation. Regression lines are from locally weighted scatterplot smoothing (LOWESS).

the lower Athabasca River. These hydrological effects would in turn alter spatial patterns of PAD water bodies, vegetation, habitat, and ecosystems as changes to inundation frequency influence plant succession over large areas (Prowse et al., 1996). There could also be negative impacts on Indigenous people cultural and traditional activities (e.g., fishing, trapping, hunting, and navigation). Future research should apply hydraulic avulsion

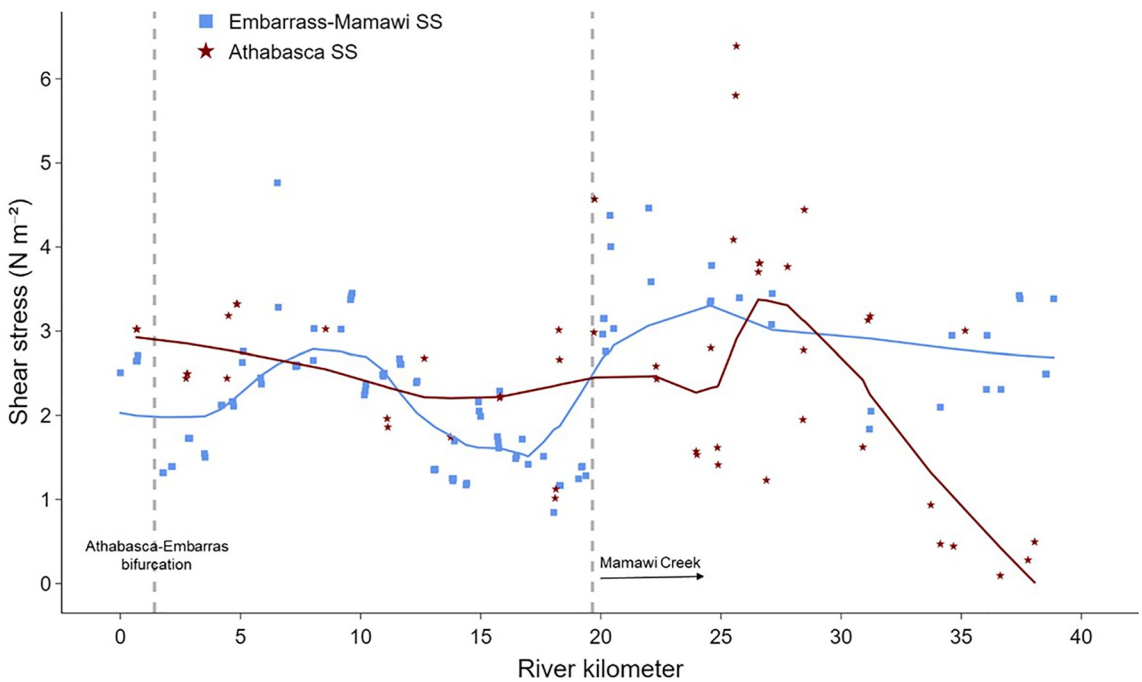

Figure 12. Longitudinal profiles of bed shear stress (τ) along the Athabasca River and the Embarras-Mamawi channel downstream of the Athabasca-Embarras bifurcation. Regression lines are from locally weighted scatterplot smoothing (LOWESS).

models to the southern PAD, parameterized with field measurements of bed material, bank material, bank cohesion, and other critical variables.

Limitations of this study include knowledge gaps regarding long-term SSC, WSS dynamics, and channel bank properties. SSC measurements at ECCC gauging stations were discontinued in the 1980s. The WSS data used in this study are from one-time field surveys conducted over 7 days of moderately fluctuating discharge. The average Athabasca River discharge during these measurements was 1,124 m^{-3} s^{-1}, which is somewhat higher than the long-term average discharge of 676 m^3 s^{-1}. WSS during high flow conditions (i.e., >2,000 m^3 s^{-1}) is unknown. High-flow SSC and WSS would be particularly useful for studying sediment transport capacity and gradient advantage of the competing Athabasca and Embarras-Mamawi channels during large channel-forming events. Finally, we suspect that the observed rapid growth in surface area of both deltas from 1998 to 2003 may be related to a combination of wildfire and large backwater effects during extensive 1996–1997 flooding but cannot confirm this (Text S1 and Figures S6–S8 in Supporting Information S1). This short period of rapid delta growth overwhelms subsequent avulsion-driven contrasts and deserves further investigation. Repeated bathymetry measurements may be needed in the Mamawi Lake and Lake Athabasca to further estimate volume changes of the delta.

Regardless of these limitations, we conclude that field measurements and remote sensing support that a slow but important river avulsion is currently underway in the southern portions of the PAD, Canada. In light of its growing discharge capture and steeper flow path, the Embarras-Mamawi channel represents a plausible alternate flow course for the Athabasca River that is enlarging. An eventual capture of the Athabasca River and an associated major PAD lobe switching event cannot be ruled out, especially in light of projected future increases in Athabasca River discharge and sediment load.

The case study presented here for the PAD indicates that slow or ongoing avulsions may be identified and monitored through hydrologic measurements of WSS and discharge, together with remote sensing of channel width, floodplain inundation patterns, and downstream delta growth. The recently launched NASA Surface Water and Ocean Topography (SWOT) satellite will provide repeated global surveys of water surface elevations globally (i.e., lakes, reservoirs, wetlands, and rivers wider than 100 m) as well estimates of river discharge (Biancamaria et al., 2016). We propose that SWOT measurements of WSE, surface slope, and discharge in competing distributaries of large rivers, together with field measurements and other remotely sensed products, should aid identification of particular channels having the highest stream power, channel growth, and avulsion potential. Such information could aid studies of bifurcation stability (Pittaluga et al., 2015), future avulsion potential, and guide the development of long-term river and floodplain management strategies.

Data Availability Statement

Field measurements of water surface elevation, water depth, and ADCP data can be found at https://zenodo.org/record/7622504#.Y-PuG3bMJaQ. Landsat imagery can be downloaded at https://earthexplorer.usgs.gov/ and https://earthengine.google.com/. Long-term river stage and discharge data for the studied rivers can be downloaded at https://wateroffice.ec.gc.ca/map/index_e.html.

Acknowledgments
This research was funded by the NASA Surface Water and Ocean Topography mission (Grant 80NSSC20K1144S), managed by Dr. Nadya Vinogradova-Shiffer. We would like to thank Queenie Gray and Wood Buffalo National Park for enabling our field visits. We would also like to thank Robert and Barbara Grandjambe for guiding and boat piloting services during the field measurements.

References

Allen, G. H., & Pavelsky, T. M. (2018). Global extent of rivers and streams. *Science*, *361*(6402), 585–588. https://doi.org/10.1126/science.aat0636

Allen, J. R. L. (1965). A review of the origin and characteristics of recent alluvial sediments. *Sedimentology*, *5*(2), 89–191. https://doi.org/10.1111/j.1365-3091.1965.tb01561.x

Ashworth, P. J., Best, J. L., & Jones, M. (2004). Relationship between sediment supply and avulsion frequency in braided rivers. *Geology*, *32*(1), 21–24. https://doi.org/10.1130/g19919.1

Aslan, A., Autin, W. J., & Blum, M. D. (2005). Causes of River Avulsion: Insights from the late Holocene avulsion history of the Mississippi River, U.S.A. *Journal of Sedimentary Research*, *75*(4), 650–664. https://doi.org/10.2110/jsr.2005.053

Babaeyan-Koopaei, K., Ervine, D. A., Carling, P. A., & Cao, Z. (2002). Velocity and turbulence measurements for two overbank flow events in River Severn. *Journal of Hydraulic Engineering*, *128*(10), 891–900. https://doi.org/10.1061/(ASCE)0733-9429(2002)128:10(891)

Bagnold, R. A. (1960). Sediment discharge and stream power—A preliminary announcement, report 421.

Bagnold, R. A. (1966). An approach to the sediment transport problem from general physics, report 422I.

Bayrock, L. A., & Root, J. D. (1972). *Geology of the Peace-Athabasca River Delta region, Alberta Report* (p. 58). Alberta Research Council, ARC/AGS Open File Report.

Beltaos, S. (2023). The drying peace–Athabasca Delta, Canada: Review and synthesis of cryo-hydrologic controls and projections to future climatic conditions. *Sustainability*, *15*(3), 2103. https://doi.org/10.3390/su15032103

Beltaos, S., Prowse, T., Bonsal, B., MacKay, R., Romolo, L., Pietroniro, A., & Toth, B. (2006). Climatic effects on ice-jam flooding of the Peace-Athabasca Delta. *Hydrological Processes*, *20*(19), 4031–4050. https://doi.org/10.1002/hyp.6418

Beltaos, S., Prowse, T. D., & Carter, T. (2006). Ice regime of the lower Peace River and ice-jam flooding of the Peace-Athabasca Delta. *Hydrological Processes*, *20*(19), 4009–4029. https://doi.org/10.1002/hyp.6417

Bentley, S. J., Blum, M. D., Maloney, J., Pond, L., & Paulsell, R. (2016). The Mississippi River source-to-sink system: Perspectives on tectonic, climatic, and anthropogenic influences, Miocene to Anthropocene. *Earth-Science Reviews*, *153*, 139–174. https://doi.org/10.1016/j.earscirev.2015.11.001

Biancamaria, S., Lettenmaier, D. P., & Pavelsky, T. M. (2016). The SWOT mission and its capabilities for land hydrology. *Surveys in Geophysics*, *37*(2), 307–337. https://doi.org/10.1007/s10712-015-9346-y

Brooke, S., Chadwick, A. J., Silvestre, J., Lamb, M. P., Edmonds, D. A., & Ganti, V. (2022). Where rivers jump course. *Science*, *376*(6596), 987–990. https://doi.org/10.1126/science.abm1215

Bryant, M., Falk, P., & Paola, C. (1995). Experimental study of avulsion frequency and rate of deposition. *Geology*, *23*(4), 365–368. https://doi.org/10.1130/0091-7613(1995)023<0365:ESOAFA>2.3.CO;2

Buehler, H. A., Weissmann, G. S., Scuderi, L. A., & Hartley, A. J. (2011). Spatial and temporal evolution of an avulsion on the Taquari River distributive fluvial system from satellite image analysis. *Journal of Sedimentary Research*, *81*(8), 630–640. https://doi.org/10.2110/jsr.2011.040

Chadwick, A. J., Lamb, M. P., & Ganti, V. (2020). Accelerated river avulsion frequency on lowland deltas due to sea-level rise. *Proceedings of the National Academy of Sciences*, *117*(30), 17590. https://doi.org/10.1073/pnas.1912351117

Chen, Y., Syvitski, J. P. M., Gao, S., Overeem, I., & Kettner, A. J. (2012). Socio-economic impacts on flooding: A 4000-year history of the Yellow River, China. *AMBIO*, *41*(7), 682–698. https://doi.org/10.1007/s13280-012-0290-5

Correggiari, A., Cattaneo, A., & Trincardi, F. (2005). The modern Po Delta system: Lobe switching and asymmetric prodelta growth. *Marine Geology*, *222–223*, 49–74. https://doi.org/10.1016/j.margeo.2005.06.039

Dibike, Y., Shakibaeinia, A., Eum, H. I., Prowse, T., & Droppo, I. (2018). Effects of projected climate on the hydrodynamic and sediment transport regime of the lower Athabasca River in Alberta, Canada. *River Research and Applications*, *34*(5), 417–429. https://doi.org/10.1002/rra.3273

Donselaar, M. E., Cuevas Gozalo, M. C., & Moyano, S. (2013). Avulsion processes at the terminus of low-gradient semi-arid fluvial systems: Lessons from the Río Colorado, Altiplano endorheic basin, Bolivia. *Sedimentary Geology*, *283*, 1–14. https://doi.org/10.1016/j.sedgeo.2012.10.007

Edmonds, D. A., Hajek, E. A., Downton, N., & Bryk, A. B. (2016). Avulsion flow-path selection on rivers in foreland basins. *Geology*, *44*(9), 695–698. https://doi.org/10.1130/g38082.1

Edmonds, D. A., Hoyal, D. C. J. D., Sheets, B. A., & Slingerland, R. L. (2009). Predicting delta avulsions: Implications for coastal wetland restoration. *Geology*, *37*(8), 759–762. https://doi.org/10.1130/G25743A.1

Ethridge, F. G., Skelly, R. L., & Bristow, C. S. (1999). Avulsion and crevassing in the sandy, braided Niobrara River: Complex response to base-level rise and aggradation. In *Fluvial sedimentology VI* (pp. 179–191). https://doi.org/10.1002/9781444304213.ch14

Eum, H.-I., Dibike, Y., & Prowse, T. (2017). Climate-induced alteration of hydrologic indicators in the Athabasca River Basin, Alberta, Canada. *Journal of Hydrology*, *544*, 327–342. https://doi.org/10.1016/j.jhydrol.2016.11.034

Fisk, H. N. (1944). *Geological investigation of the alluvial valley of the lower Mississippi River* (p. 78.). U.S. Department of the Army, Mississippi River Commission Report.

Ganti, V., Chadwick, A. J., Hassenruck-Gudipati, H. J., & Lamb, M. P. (2016). Avulsion cycles and their stratigraphic signature on an experimental backwater-controlled delta. *Journal of Geophysical Research: Earth Surface*, *121*(9), 1651–1675. https://doi.org/10.1002/2016JF003915

Gartner, J. D., Dade, W. B., Renshaw, C. E., Magilligan, F. J., & Buraas, E. M. (2015). Gradients in stream power influence lateral and downstream sediment flux in floods. *Geology*, *43*(11), 983–986. https://doi.org/10.1130/g36969.1

Gradziński, R., Baryła, J., Doktor, M., Gmur, D., Gradziński, M., Kędzior, A., et al. (2003). Vegetation-controlled modern anastomosing system of the upper Narew River (NE Poland) and its sediments. *Sedimentary Geology*, *157*(3), 253–276. https://doi.org/10.1016/S0037-0738(02)00236-1

Hajek, E., & Edmonds, D. (2014). Is river avulsion style controlled by floodplain morphodynamics? *Geology*, *42*(3), 199–202. https://doi.org/10.1130/G35045.1

Harlan, M. E., Gleason, C. J., Altenau, E. H., Butman, D., Carter, T., Chu, V. W., et al. (2021). Discharge estimation from dense arrays of pressure transducers. *Water Resources Research*, *57*(3), e2020WR028714. https://doi.org/10.1029/2020wr028714

Iacobucci, G., Troiani, F., Milli, S., Mazzanti, P., Piacentini, D., Zocchi, M., & Nadali, D. (2020). Combining satellite multispectral imagery and topographic data for the detection and mapping of fluvial avulsion processes in lowland areas. *Remote Sensing*, *12*(14), 2243. https://doi.org/10.3390/rs12142243

Jensen, J. R. (2008). Remote sensing of the environment: An earth resource perspective, Pearson Education, [Delhi, India].

Jerolmack, D. J., & Paola, C. (2007). Complexity in a cellular model of river avulsion. *Geomorphology*, *91*(3–4), 259–270. https://doi.org/10.1016/j.geomorph.2007.04.022

Jones, L. S., & Harper, J. T. (1998). Channel avulsions and related processes, and large-scale sedimentation patterns since 1875, Rio Grande, San Luis Valley, Colorado. *The Geological Society of America Bulletin*, *110*(4), 411–421. https://doi.org/10.1130/0016-7606(1998)110<0411:Caarpa>2.3.Co;2

Jones, L. S., & Schumm, S. A. (1999). Causes of Avulsion: An Overview. In N. D. Smith & J. C. Roger (Eds.), *Fluvial sedimentology VI* (pp. 169–178). https://doi.org/10.1002/9781444304213.ch13

Kay, M. L., Wiklund, J. A., Remmer, C. R., Neary, L. K., Brown, K., Ghosh, A., et al. (2019). Bi-directional hydrological changes in perched basins of the Athabasca Delta (Canada) in recent decades caused by natural processes. *Environmental Research Communications*, *1*(8), 081001. https://doi.org/10.1088/2515-7620/ab37e7

Kendall, M. G. (1975). *Rank correlation methods*. Griffin.

Kleinhans, M. G., Jagers, H. R. A., Mosselman, E., & Sloff, C. J. (2008). Bifurcation dynamics and avulsion duration in meandering rivers by one-dimensional and three-dimensional models. *Water Resources Research*, *44*(8), W08454. https://doi.org/10.1029/2007wr005912

Lauzon, R., & Murray, A. B. (2022). Discharge determines avulsion regime in model experiments with vegetated and unvegetated deltas. *Journal of Geophysical Research: Earth Surface*, *127*(2), e2021JF006225. https://doi.org/10.1029/2021jf006225

Li, J. G., Yang, X. C., Maffei, C., Tooth, S., & Yao, G. Q. (2018). Applying independent component analysis on Sentinel-2 imagery to characterize geomorphological responses to an extreme flood event near the non-vegetated Rio Colorado terminus, Salar de Uyuni, Bolivia. *Remote Sensing*, *10*(5), 725. https://doi.org/10.3390/rs10050725

Lombardo, U. (2016). Alluvial plain dynamics in the southern Amazonian foreland basin. *Earth System Dynamics*, *7*(2), 453–467. https://doi.org/10.5194/esd-7-453-2016

Louzada, R. O., Bergier, I., Roque, F. O., McGlue, M. M., Silva, A., & Assine, M. L. (2021). Avulsions drive ecosystem services and economic changes in the Brazilian Pantanal wetlands. *Current Research in Environmental Sustainability*, *3*, 100057. https://doi.org/10.1016/j.crsust.2021.100057

Mackey, S. D., & Bridge, J. S. C. (1995). Three-dimensional model of alluvial stratigraphy; theory and applications. *Journal of Sedimentary Research*, *65*(1b), 7–31. https://doi.org/10.1306/d42681d5-2b26-11d7-8648000102c1865d
Makaske, B., Maathuis, B. H. P., Padovani, C. R., Stolker, C., Mosselman, E., & Jongman, R. H. G. (2012). Upstream and downstream controls of recent avulsions on the Taquari megafan, Pantanal, south-western Brazil. *Earth Surface Processes and Landforms*, *37*(12), 1313–1326. https://doi.org/10.1002/esp.3278
Mann, H. B. (1945). Nonparametric tests against trend. *Econometrica*, *13*(3), 245–259. https://doi.org/10.2307/1907187
Mohrig, D., Heller, P. L., Paola, C., & Lyons, W. J. (2000). Interpreting avulsion process from ancient alluvial sequences: Guadalope-Matarranya system (northern Spain) and Wasatch Formation (western Colorado). *The Geological Society of America Bulletin*, *112*(12), 1787–1803. https://doi.org/10.1130/0016-7606(2000)112<1787:Iapfaa>2.0.Co;2
Nanson, G. C., & Knighton, A. D. (1996). Anabranching rivers: Their cause, character and classification. *Earth Surface Processes and Landforms*, *21*(3), 217–239. https://doi.org/10.1002/(sici)1096-9837(199603)21:3<217::Aid-esp611>3.0.Co;2-u
Pavelsky, T. M., & Smith, L. C. (2008). Remote sensing of hydrologic recharge in the Peace-Athabasca Delta, Canada. *Geophysical Research Letters*, *35*(8), L08403. https://doi.org/10.1029/2008gl033268
Pavelsky, T. M., & Smith, L. C. (2009). Remote sensing of suspended sediment concentration, flow velocity, and lake recharge in the Peace-Athabasca Delta, Canada. *Water Resources Research*, *45*(11), W11417. https://doi.org/10.1029/2008wr007424
Pekel, J.-F., Cottam, A., Gorelick, N., & Belward, A. S. (2016). High-resolution mapping of global surface water and its long-term changes. *Nature*, *540*(7633), 418–422. https://doi.org/10.1038/nature20584
Peters, D. L., Prowse, T. D., Pietroniro, A., & Leconte, R. (2006). Flood hydrology of the Peace-Athabasca Delta, northern Canada. *Hydrological Processes*, *20*(19), 4073–4096. https://doi.org/10.1002/hyp.6420
Peters, D. L., Watt, D., Devito, K., Monk, W. A., Shrestha, R. R., & Baird, D. J. (2022). Changes in geographical runoff generation in regions affected by climate and resource development: A case study of the Athabasca River. *Journal of Hydrology: Regional Studies*, *39*, 100981. https://doi.org/10.1016/j.ejrh.2021.100981
Phillips, J. D. (2009). Avulsion regimes in southeast Texas rivers. *Earth Surface Processes and Landforms*, *34*(1), 75–87. https://doi.org/10.1002/esp.1692
Phillips, J. D. (2012). Log-jams and avulsions in the San Antonio River Delta, Texas. *Earth Surface Processes and Landforms*, *37*(9), 936–950. https://doi.org/10.1002/esp.3209
Pittaluga, M. B., Coco, G., & Kleinhans, M. G. (2015). A unified framework for stability of channel bifurcations in gravel and sand fluvial systems. *Geophysical Research Letters*, *42*(18), 7521–7536. https://doi.org/10.1002/2015gl065175
Prasojo, O. A., Hoey, T. B., Owen, A., & Williams, R. D. (2022). Slope break and avulsion locations scale consistently in global deltas. *Geophysical Research Letters*, *49*(2), e2021GL093656. https://doi.org/10.1029/2021GL093656
Prowse, T. D., Aitken, B., Demuth, M. N., & Peterson, M. (1996). Strategies for restoring spring flooding to a drying northern delta. *Regulated Rivers: Research & Management*, *12*(2–3), 237–250. https://doi.org/10.1002/(sici)1099-1646(199603)12:2/3<237::Aid-rrr392>3.3.Co;2-b
Prowse, T. D., & Conly, F. M. (1998). Effects of climatic variability and flow regulation on ice-jam flooding of a northern delta. *Hydrological Processes*, *12*(10–11), 1589–1610. https://doi.org/10.1002/(sici)1099-1085(199808/09)12:10/11<1589::Aid-hyp683>3.3.Co;2-7
Prowse, T. D., & Lalonde, V. (1996). Open-Water and ice-jam flooding of a Northern Delta: Paper presented at the 10th northern res. basin symposium (Svalbard, Norwa—28 Aug./3 Sept. 1994). *Hydrology Research*, *27*(1–2), 85–100. https://doi.org/10.2166/nh.1996.0021
Qian, N. (1990). Fluvial processes in the lower Yellow River after levee breaching at Tongwaxiang in 1855. *International Journal of Sediment Research*, *5*(2), 1–13.
Ratliff, K. M., Hutton, E. W. H., & Murray, A. B. (2021). Modeling long-term delta dynamics reveals persistent geometric river avulsion locations. *Earth and Planetary Science Letters*, *559*, 116786. https://doi.org/10.1016/j.epsl.2021.116786
Richards, K. S. (1982). *Rivers, form and process in alluvial channels*. Methuen.
Roberts, H. H., Coleman, J. M., Bentley, S. J., & Walker, N. (2003). An embryonic major delta lobe; a new generation of delta studies in the Atchafalaya-Wax Lake delta system. *Transactions: Gulf Coast Association of Geological Societies*, *53*, 690–703.
Rosen, T., & Xu, Y. J. (2013). Recent decadal growth of the Atchafalaya River Delta complex: Effects of variable riverine sediment input and vegetation succession. *Geomorphology*, *194*, 108–120. https://doi.org/10.1016/j.geomorph.2013.04.020
Schumm, S. A., Erskine, W. D., & Tilleard, J. W. (1996). Morphology, hydrology, and evolution of the anastomosing Ovens and King Rivers, Victoria, Australia. *The Geological Society of America Bulletin*, *108*(10), 1212. https://doi.org/10.1130/0016-7606(1996)108<1212:mhaeot>2.3.co;2
Sinha, R. (2009). The Great avulsion of Kosi on 18 August 2008. *Current Science*, *97*(3), 429–433.
Sinha, R., Sripriyanka, K., Jain, V., & Mukul, M. (2014). Avulsion threshold and planform dynamics of the Kosi River in north Bihar (India) and Nepal: A GIS framework. *Geomorphology*, *216*, 157–170. https://doi.org/10.1016/j.geomorph.2014.03.035
Slingerland, R., & Smith, N. D. (1998). Necessary conditions for a meandering-river avulsion. *Geology*, *26*(5), 435–438. https://doi.org/10.1130/0091-7613(1998)026<0435:NCFAMR>2.3.CO;2
Slingerland, R., & Smith, N. D. (2004). River avulsions and their deposits. *Annual Review of Earth and Planetary Sciences*, *32*(1), 257–285. https://doi.org/10.1146/annurev.earth.32.101802.120201
Smith, D. G. (1994). Glacial Lake McConnell: Paleogeography, age, duration, and associated river deltas, Mackenzie River basin, western Canada. *Quaternary Science Reviews*, *13*(9), 829–843. https://doi.org/10.1016/0277-3791(94)90004-3
Smith, D. G. (2003). 1100 years of ice-jam flooding in the Peace River Delta interpreted from flood bed sediments and ice-scarred trees report.
Smith, L. C. (2020). *Rivers of power: How a natural force raised kingdoms, destroyed civilizations, and shapes our world*. Little Brown Spark/Hachette Book Group.
Smith, N. D., Cross, T. A., Dufficy, J. P., & Clough, S. R. (1989). Anatomy of an avulsion. *Sedimentology*, *36*(1), 1–23. https://doi.org/10.1111/j.1365-3091.1989.tb00817.x
Smith, N. D., Morozova, G. S., & Gibling, M. R. (2014). Channel enlargement by avulsion-induced sediment starvation in the Saskatchewan River. *Geology*, *42*(4), 355–358. https://doi.org/10.1130/g35258.1
Smith, N. D., Slingerland, R. L., Pérez-Arlucea, M., & Morozova, G. S. (1998). The 1870s avulsion of the Saskatchewan River. *Canadian Journal of Earth Sciences*, *35*(4), 453–466. https://doi.org/10.1139/e97-113
Stouthamer, E., & Berendsen, H. J. A. (2001). Avulsion frequency, avulsion duration, and interavulsion period of Holocene channel belts in the Rhine-Meuse Delta, the Netherlands. *Journal of Sedimentary Research*, *71*(4), 589–598. https://doi.org/10.1306/112100710589
Sun, T., Paola, C., Parker, G., & Meakin, P. (2002). Fluvial fan deltas: Linking channel processes with large-scale morphodynamics. *Water Resources Research*, *38*(8), 26-1–26-10. https://doi.org/10.1029/2001wr000284
Timoney, K. (2002). A dyin delta? A case study of a wetland paradigm. *Wetlands*, *22*(2), 282–300. https://doi.org/10.1672/0277-5212(2002)022[0282:addacs]2.0.co;2
Timoney, K. (2013). *The Peace-Athabasca delta: Portrait of a dynamic ecosystem*. The University of Alberta Press.

Timoney, K., & Lee, P. (2016). Changes in the areal extents of the Athabasca River, Birch River, and Cree Creek Deltas, 1950–2014, Peace-Athabasca Delta, Canada. *Geomorphology*, *258*, 95–107. https://doi.org/10.1016/j.geomorph.2016.01.011

Timoney, K. P. (2021). Flooding in the Peace-Athabasca Delta: Climatic and hydrologic change and variation over the past 120 years. *Climatic Change*, *169*(3–4), 26. https://doi.org/10.1007/s10584-021-03257-z

Tornqvist, T. E. (1994). Middle and late Holocene avulsion history of the River Rhine (Rhine-Meuse delta, Netherlands). *Geology*, *22*(8), 711–714. https://doi.org/10.1130/0091-7613(1994)022<0711:malhah>2.3.co;2

Törnqvist, T. E., & Bridge, J. S. (2002). Spatial variation of overbank aggradation rate and its influence on avulsion frequency. *Sedimentology*, *49*(5), 891–905. https://doi.org/10.1046/j.1365-3091.2002.00478.x

Toyra, J., Pietroniro, A., Martz, L. W., & Prowse, T. D. (2002). A multi-sensor approach to wetland flood monitoring. *Hydrological Processes*, *16*(8), 1569–1581. https://doi.org/10.1002/hyp.1021

Valenza, J. M., Edmonds, D. A., Hwang, T., & Roy, S. (2020). Downstream changes in river avulsion style are related to channel morphology. *Nature Communications*, *11*(1), 2116. https://doi.org/10.1038/s41467-020-15859-9

Vespremeanu-Stroe, A., Zainescu, F., Preoteasa, L., Tatui, F., Rotaru, S., Morhange, C., et al. (2017). Holocene evolution of the Danube delta: An integral reconstruction and a revised chronology. *Marine Geology*, *388*, 38–61. https://doi.org/10.1016/j.margeo.2017.04.002

Wang, B., & Xu, Y. J. (2018). Decadal-scale riverbed deformation and sand budget of the last 500 km of the Mississippi River: Insights Into natural and river engineering effects on a large Alluvial River. *Journal of Geophysical Research: Earth Surface*, *123*(5), 874–890. https://doi.org/10.1029/2017JF004542

Wang, B., Xu, Y. J., Xu, W., Cheng, H., Chen, Z., & Zhang, W. (2020). Riverbed changes of the uppermost Atchafalaya River, USA—A case study of channel dynamics in large man-controlled alluvial river confluences. *Water*, *12*(8), 2139. https://doi.org/10.3390/w12082139

Weissmann, G. S., Hartley, A. J., Scuderi, L. A., Nichols, G. J., Owen, A., Wright, S., et al. (2015). Fluvial geomorphic elements in modern sedimentary basins and their potential preservation in the rock record: A review. *Geomorphology*, *250*, 187–219. https://doi.org/10.1016/j.geomorph.2015.09.005

Wolfe, B. B., Hall, R. I., Last, W. M., Edwards, T. W. D., English, M. C., Karst-Riddoch, T. L., et al. (2006). Reconstruction of multi-century flood histories from oxbow lake sediments, Peace-Athabasca Delta, Canada. *Hydrological Processes*, *20*(19), 4131–4153. https://doi.org/10.1002/hyp.6423

Xu, H. (2006). Modification of normalised difference water index (NDWI) to enhance open water features in remotely sensed imagery. *International Journal of Remote Sensing*, *27*(14), 3025–3033. https://doi.org/10.1080/01431160600589179

Xue, C. (1993). Historical changes in the Yellow River delta, China. *Marine Geology*, *113*(3), 321–330. https://doi.org/10.1016/0025-3227(93)90025-Q

Yang, C. T. (1979). Unit stream power equations for total load. *Journal of Hydrology*, *40*(1–2), 123–138. https://doi.org/10.1016/0022-1694(79)90092-1

Yang, X., Pavelsky, T. M., Allen, G. H., & Donchyts, G. (2020). RivWidthCloud: An automated Google Earth engine algorithm for river width extraction from remotely sensed imagery. *IEEE Geoscience and Remote Sensing Letters*, *17*(2), 217–221. https://doi.org/10.1109/lgrs.2019.2920225

Yochum, S. E., Sholtes, J. S., Scott, J. A., & Bledsoe, B. P. (2017). Stream power framework for predicting geomorphic change: The 2013 Colorado Front Range flood. *Geomorphology*, *292*, 178–192. https://doi.org/10.1016/j.geomorph.2017.03.004

Zhang, X., & Fang, X. (2017). Temporal and spatial variation of catastrophic river floodings in the Lower Yellow River from AD 960 to 1938. *The Holocene*, *27*(9), 1359–1369. https://doi.org/10.1177/0959683617690590

References From the Supporting Information

Long, C. M., & Pavelsky, T. M. (2013). Remote sensing of suspended sediment concentration and hydrologic connectivity in a complex wetland environment. *Remote Sensing of Environment*, *129*, 197–209. https://doi.org/10.1016/j.rse.2012.10.019

Malmon, D. V., Reneau, S. L., Katzman, D., Lavine, A., & Lyman, J. (2007). Suspended sediment transport in an ephemeral stream following wildfire. *Journal of Geophysical Research*, *112*(F2), F02006. https://doi.org/10.1029/2005JF000459